Study on Synthesis and Characterization of Ferromagnetic Cubic Perovskite Oxides Containing Co^{4+} Ion.

By

Hideki TAGUCHI

Contents

Chapter 1	INTRODUCTION	1
Chapter 2	EXPERIMENTAL PROCEDURE	14
2-1)	High oxygen pressure apparatus	14
2-2)	X-ray diffraction	14
2-3)	Chemical analysis	16
2-4)	Magnetic measurement	16
2-5)	Electrical conductivity measurement	18
2-6)	Mössbauer effect measurement	18
Chapter 3	EXPERIMENTAL RESULTS	19
3-1)	$SrCoO_{3-\delta}$ system	19
3-2)	$(La_{1-X}Sr_X)CoO_3$ system	36
3-3)	$Sr(Co_{1-X}Mn_X)O_3$ system	48
Chapter 4	DISCUSSION	61
4-1)	$SrCoO_{3-\delta}$ system	61
4-2)	$(La_{1-X}Sr_X)CoO_3$ system	74
4-3)	$Sr(Co_{1-X}Mn_X)O_3$ system	83
4-4)	Co^{4+} ion at octahedral environment	90
SUMMARY		97
ACKNOWLEDGMENTS		100
REFERENCES		101

Chapter 1. INTRODUCTION

In the oxides containing the tetravalent state of the first row transition metal ions, $M^{4+}O_2$ (M: Ti, V, Cr, and Mn) oxides with rutil structure are well known and their physical properties are also systematically examined. In the oxides containing Fe, Co and Ni ions, however, these ions are normally in di- or tri-valent state, but a tetravalent state of Fe, Co and Ni ions only exists in the oxides with perovskite structure in $SrFe^{4+}O_3$ (1), $SrCo^{4+}O_3$ (2) and $BaNi^{4+}O_3$ (3), whose chemical formula are generally presented as $A^{2+}B^{4+}O_3$ (A: alkaline earth metal, B: transition metal).

Since Yakel synthesized $SrFe^{4+}O_3$ and $SrCo^{4+}O_3$ (4), the magnetic and electrical properties of oxides containing the tetravalent state ions such as Fe^{4+}, Co^{4+} and Ni^{4+} ions have been investigated by many investigators (1,2,3, 4,5,6,7)

The perovskite structure (ABO_3) has the cubic unit cell with the space group Pm3m. Large A cation and oxygen ions are packed with f.c.c. (face centered cubic) and small B cation locates at the spaces. Large A cation is surrounded by twelve oxygen ions and B cation is surrounded by six oxygen ions as shown in Fig. 1. The octahedron containing B cations are connected at the corners each other and the angle of B-O-B is 180°. Considering the

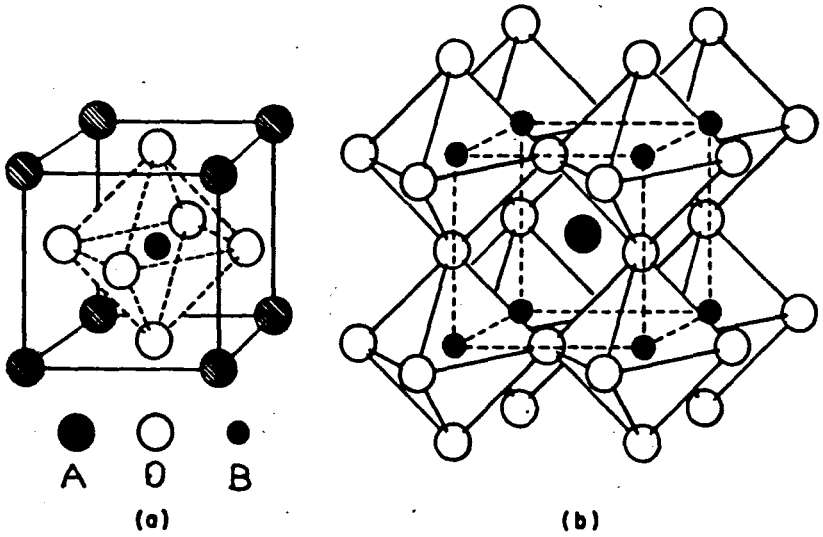

Fig. 1 Structure of cubic perovskite (ABO_3).

ideal packing between these three ions in the perovskite structure (ABO_3), Goldshmidt defined the tolerable limits on the size of A cation via a tolerance factor (t),

$$t=(r_A+r_0)/\sqrt{2}(r_B+r_0) \quad \text{--- (1)}$$

where r_A, r_B and r_0 are empirical radii of the respective ions. Although the ideal cubic perovskite structure should have t=1, the perovskite structure often occurs only within the value between 0.75 and 1.0.

Table 1 shows the crystallographic, magnetic and electrical properties of the perovskite type oxides containing the tetravalent state of the first row transition metals such as Ti^{4+}, V^{4+}, Cr^{4+} Mn^{4+}, Fe^{4+} and Co^{4+} ions.

Ti^{4+} ion has no 3d electrons ($3d^0$). The titanates such as $BaTiO_3$ and $SrTiO_3$ exhibit paramagnetism (8). These oxides are used as the end-member of solid solution systems to investigate the dilution effects on the physical properties of another kind of tetravalent state transition metal ions such as the system $SrTiO_3$-$SrFeO_3$ (9).

Perovskite type metavanadates, $CaVO_3$ and $SrVO_3$, were prepared under high pressures by Chamberland et al. (10). $CaVO_3$ has an orthorhombic distorted perovskite structure with a=0.5422 nm, b=0.5335 nm and c=0.7541 nm. $CaVO_3$ shows Pauli paramagnetic behavior and exhibits metallic conductivity. $SrVO_3$ has a cubic structure with a=0.3842 nm. $SrVO_3$ also shows Pauli paramagnetic behavior

Table 1 Cell constants, magnetic and electrical properties of perovskite type oxides.

oxide	cell constant	magnetic property	electrical property	ref.
$BaTiO_3$	a=0.3994 nm, c=0.4038 nm	para.		8
$SrTiO_3$	a=0.3905 nm	para.		8
$CaVO_3$	a=0.5422 nm, b=0.5335 nm c=0.7541 nm	Pauli para.	metallic	10
$SrVO_3$	a=0.3842 nm	Pauli para.	metallic	10
$CaCrO_3$	a=0.5287 nm, b=0.5316 nm c=0.7486 nm	weak ferro.	semicon.	12
$SrCrO_3$	a=0.3818 nm	Pauli para.	metallic	13
$CaMnO_3$	a=0.5270 nm, b=0.5275 nm c=0.7464 nm	weak ferro.	semicon.	14
$SrMnO_3$	a=0.3802 nm	antiferro.	insulator	14
$CaFeO_3$	a=0.3770 nm	antiferro.		16
$SrFeO_3$	a=0.3850 nm	antiferro.	metallic	18
$SrCoO_3$	a=0.3860 nm	ferro.	metallic	19

para.: paramagnetic ferro.: ferromagnetic

antiferro.: antiferromagnetic

and exhibits metallic conductivity. Magnetic and electrical properties of $CaVO_3$ and $SrVO_3$ are well explained by the delocalized model proposed by Goodenough for the perovskite type compounds having one electron system such as Ti^{3+} and Re^{6+} ions (11).

Metachromates, $CaCrO_3$ (12) and $SrCrO_3$ (13), were prepared under high pressures. $CaCrO_3$ has an orthorhombic distorted perovskite structure with a=0.5287 nm, c=0.5316 nm and c=0.7486 nm. It exhibits a weak ferromagnetism with T_N=90K and is semiconductor. $CaCrO_3$ is characteristic as a spontenious collective electron magnetism. On the other hand, $SrCrO_3$ has a cubic perovskite structure with a = 0.3818 nm and shows metallic and Pauli paramagnetic behaviors. Magnetic and electrical properties of $SrCrO_3$ are introduced by collective or delocalized t_{2g} electrons.

Metamanganates, $CaMnO_3$ and $SrMnO_3$, were prepared under high oxygen pressures (14). $CaMnO_3$ has an orthorhombic distorted perovskite structure with a=0.5270 nm, b=0.5275 nm and c=0.7464 nm. $CaMnO_3$ exhibits a weak ferromagnetism with T_N=123K. Electrical resistivities of 1.6 Ωcm at 298K and 3.2×10^3 Ωcm at 78K were obtained. $SrMnO_3$ has a cubic perovskite structure with a=0.3802 nm and exhibits an antiferromagnetism with T_N=260K.

From the results of the neutron diffraction study of $SrMnO_3$ (15), $SrMnO_3$ is a G-type antiferromagnetic ordering where each Mn^{4+} ion is surrounded by six Mn^{4+}

ions whose spins are antiparallel to the given ion. The magnetic moment of Mn^{4+} ion was found to be $2.6\pm0.2\ \mu_B$ at 77K. The electrical resistivity of $SrMnO_3$ is very high.

$CaFeO_3$ was first prepared at high temperature under high oxygen pressure by Kanamaru et al. (16) and is indexed as a cubic perovskite structure with a=0.3770 nm. The value of isomershift corresponding to the tetravalent state of iron is obtained from Mössbauer effect measurement at room temperature. $CaFeO_3$ is an antiferromagnetism with T_N=120K. The effective magnetic moment is $2.20\ \mu_B$. Recently Takeda et al. measured the Mössbauer spectra of $CaFeO_3$ at 4.2K (17). Mössbauer spectrum consisting of two sets magnetic hyperfine patterns with nearly the same intensities is explained assuming a charge displacement, $2Fe^{4+} \rightarrow Fe^{3+} + Fe^{5+}$.

$SrFeO_3$ was prepared at high oxygen pressures (above 30 MPa at 823K) by MacChesney (1). Application of high oxygen pressures are required to prepare both $SrFeO_3$ and $CaFeO_3$, because $Sr_2Fe_2O_5$ and $Ca_2Fe_2O_5$ with a brownmillerite structure is stable under low oxygen pressures (P_{O_2} = 0.2 MPa). $SrFeO_3$ is indexed as a cubic perovskite structure with a=0.3850 nm. $SrFeO_3$ is a good conductor ($\rho \simeq 10^{-3}\ \Omega$cm) and shows a metallic behavior. $SrFeO_3$ is antiferromagnetic below 130K. From the results of neutron diffraction study of $SrFeO_3$ (18), the magnetic structure is helical one

with a helical vector **k**: **k**//⟨111⟩. The magnetic moment of Fe^{4+} ion is $2.7\pm0.4\ \mu_B$ at liquid nitrogen temperature.

$SrCoO_3$ was prepared under high oxygen pressures above 30 MPa by Watanabe et al. (19). $SrCoO_3$ has a cubic perovskite structure with a=0.3836 nm and exhibits ferromagnetism below ca. 200K and shows a metallic conductivity in the temperature range from 77 to 300K. The results of magnetic measurement indicate that the electron configuration of Co^{4+} ions of $SrCoO_3$ is the low spin state with the $(d\varepsilon)^5(d\gamma)^0$.

The perovskite type oxides are favourable oxides to investigate the magnetic interaction of Me^{4+}-O-Me^{4+}, especially the superexchange magnetic interaction, because no other competing interaction is present.

Many solid solutions of A(Me(I),Me(II))O_3 were, therefore, prepared and their magnetic and electrical properties were examined.

Clevenger (9) synthesized the system of $Sr(Ti_{1-X}Fe_X)O_3$ and studied the crystallographic, magnetic and electrical properties to examine the magnetic interaction of Ti^{4+}-O-Fe^{4+}. These solid solution were indexed as the cubic perovskite structure. From the results of magnetic measurement, $Sr(Ti_{1-X}Fe_X)O_3$ was antiferromagnet in the range of $0.1 \leqq X \leqq 1.0$ with Néel temperature below 60K. The electrical conductivity decreases linearly with increasing Fe^{4+} ion

content. Since Ti^{4+} ion has no 3d electron ($3d^0$), the increase of T_N and electrical conductivity is caused by Fe^{4+} ion ($3d^4$).

Takeda et al. prepared the system of $Sr(Co_{1-X}Fe_X)O_3$ under various oxygen pressures and temperatures and studied crystallographic and magnetic properties (20). All samples were indexed as the cubic perovskite structure. From the result of magnetic measurement, samples were ferromagnetic in the range of $0 \leqq X \leqq 0.95$. The saturation magnetization (σ) and the paramagnetic Curie temperature (T_θ) increased in the range of $0 \leqq X \leqq 0.5$ and then decreased in the range of $0.5 \leqq X \leqq 1.0$.

$Sr(Cr_{1-X}Fe_X)O_{3-y}$ with $X>0.75$ were prepared by Bank et al. (21). Mössbauer spectra of $X=0.2$ and $X=0.3$ show that these specimens are magnetically ordered at room temperature. Two sets of six peaks at room temperature may be attributable to Fe^{3+} and Fe^{4+} ions respectively.

The solid solution series between $LnMe^{3+}O_3$ (Ln: rare earth metal, Me: the first transition metal) and $MMe^{4+}O_3$ (M: Ca, Sr or Ba) were also prepared to examine the magnetic interaction of Me^{3+}-O-Me^{4+}.

Jonker reported the magnetic properties of $(La,Ca)MnO_3$, $(La,Sr)MnO_3$ and $(La,Ba)MnO_3$ (5). In $(La_{1-X}Ca_X)MnO_3$ system, the manganite is indexed as an orthorhombic perovskite structure in the range of $0 \leqq X \leqq 0.16$ and as the cubic

perovskite structure in the range of $0.16 \leqq X \leqq 0.65$. The unit cell volume monotonously decreases with increasing X. In the cubic structure region, the manganite is ferromagnetic and the saturation magnetization at 20.4K is nearly equal to that calculated. In the system of $(La_{1-X}Sr_X)MnO_3$ and $(La_{1-X}Ba_X)MnO_3$, these manganites are also indexed as the cubic perovskite structures and show ferromagnetism. The values of the magnetic superexchange interaction of Mn^{3+}-O-Mn^{3+}, Mn^{3+}-O-Mn^{4+} and Mn^{4+}-O-Mn^{4+} were calculated using the compositional dependence of T_θ in these system. The following results were obtained.

$$Mn^{3+}\text{-O-}Mn^{3+} \sim 180K$$
$$Mn^{3+}\text{-O-}Mn^{4+} \sim 760K$$
$$Mn^{4+}\text{-O-}Mn^{4+} \sim -225K$$

Since the Mn^{3+}-O-Mn^{4+} magnetic interaction is positive and is very strong, the manganites exhibit ferromagnetism in the range of $0.15 \leqq X \leqq 0.4$ for $(La_{1-X}Ca_X)MnO_3$ and $0.15 \leqq X \leqq 0.45$ for $(La_{1-X}Sr_X)MnO_3$.

In the case of cobaltites, $(La_{1-X}Sr_X)CoO_3$ were synthesized in the range of $0 \leqq X \leqq 0.5$ and their crystallographic, magnetic and electrical properties (22,23,24,25) were studied. $LaCoO_3$ (26) shows a small rhombohedral deviation from the cubic form, with a=0.382 nm and $\alpha = 90°42'$. This deviation decreases with increasing Sr content and at about 50 % Sr the X-ray diffraction pattern no longer show a splitting up of the lines. Though $LaCoO_3$ is antiferromagnetic,

the cobaltite having X=ca. 0.05 were ferromagnetic. The temperature dependence of paramagnetic susceptibility obeyed the Curie-Weiss law and the paramagnetic Curie temperature (T_θ) changed from a negative to a positive value around X=0.05. The compositional dependence of Tc changed discontiniously in the range of $0.1 \leqq X \leqq 0.15$, and there is a large temperature interval between T_θ and Tc for $0.15 \leqq X \leqq 0.3$. Goodenough assumed that the covalent mixing between the transition metal d orbital and the oxygen 2P orbitals may enhance the superexchange interaction to break down the condition for localized d electrons (23). Bhide et al. measured the temperature dependence of Mössbauer spectra of $(La_{1-X}Sr_X)CoO_3$ in the ferromagnetic region (27). Sr-rich ion cluster coexists with the paramagnetic La-rich ion region in the same crystallographic phase. The 3d hole created by Sr ion substitution are itinerant above and below Tc and all the experimental data of $(La_{1-X}Sr_X)CoO_3$ ($0 \leqq X \leqq 0.5$) were explained on the basis of itinerant-electron magnetization.

Much interest has been paid to the nonstoichiometric perovskite oxides ($ABO_{3-\delta}$), because both Me^{3+} and Me^{4+} ions coexist at the octahedral site of oxides. Anion deficient nonstoichiometry has been reported on $SrFeO_{3-\delta}$, $SrMnO_{3-\delta}$ etc..

MacChesney et al. extensively examined electrical

and magnetic properties of $SrFeO_{3-\delta}$ (1). A series of strontium ferrate with a compositional range from $SrFeO_{2.7}$ to $SrFeO_{3.0}$ have been produced under oxygen pressures ranging from 0.2 to 85.5 MPa. Stoichiometric $SrFeO_{3.0}$ has a cubic perovskite structure and shows a metallic conductivity. The results of magnetic measurement indicated that $SrFeO_{3.0}$ is antiferromagnetic below 130K. With increasing oxygen deficiency, cell constants of samples increase and eventually tetragonal distortion occurs. Besides the Néel temperature decreases and the electrical resistivity increases with increasing oxygen deficiency. The Mössbauer spectra of $SrFeO_{3-\delta}$ were measured by Gallagher et al. (28) in various temperature regions. The results of isomershift indicate an electron charge at nucleus much smaller than that predicated by theoretical calculation assuming a purely ionic model. From these results, the conduction in $SrFeO_{3.0}$ must involve the oxygen ions which are separeted by only 0.193 nm from the iron ions, and might be thought to arise from covalent π bonding via mixing of iron t_{2g} and oxygen $P\pi$ orbitals. As anion deficiency is reduced leading to higher Fe^{4+} ion content and decreased lattice spacing, the energy spacing between the iron t_{2g} and oxygen $P\pi$ orbitals is reduced giving a reduced activation energy. At the composition $SrFeO_{3.0}$, there is a sufficient mixing of these orbitals to form a band of collective electron

states. The narrow conduction band thus formed would exhibit metallic conductivity, in which mobility was low. Anion vacancies would tend to decouple the system and weaken the magnetic exchange interaction, resulting in lowering Néel temperature.

The magnetic and electrical properties of perovskite oxides are strongly affected by the valence state of transition metal ion such as Me^{3+} and Me^{4+}. In order to discusse the magnetic interaction of Me^{3+}-O-Me^{3+}, Me^{3+}-O-Me^{4+} and Me^{4+}-O-Me^{4+}, it is important to examine the electron configuration of transition metal ion located at the octahedral site in perovskite oxide of which the oxygen deficiency is controlled.

From the above view-point, studies on the synthesis and the characterization of ferromagnetic cubic perovskite oxides containing Co ions were initiated by the author. In the first stage, research has been performed on the nonstoichiometric perovskite type $SrCoO_{3-\delta}$, in which the ratio of Co^{3+}/Co^{4+} is systematically changed. Annealing of $SrCoO_{3-\delta}$ under various oxygen pressures was performed, in order to obtain the best samples with the controlled oxygen deficiency and the magnetic properties were measured to investigate both the electron configuration of Co^{3+} and Co^{4+} ions and the magnetic superexchange interaction of Co^{3+}-O-Co^{3+}, Co^{3+}-O-Co^{4+} and Co^{4+}-O-Co^{4+}.

In the second course of the present research, perovskite type $(La_{1-X}Sr_X)CoO_3$ was synthesized in the range of $0.5 \leqq X \leqq 1.0$ under high oxygen pressures, and the magnetic properties were measured to study the electron configuration of Co ions and the magnetic superexchange interaction between Co^{3+} and Co^{4+} ions.

Then, perovskite type $Sr(Co_{1-X}Mn_X)O_3$ was synthesized under high oxygen pressures and the magnetic properties were measured to examine the electron configuration of Co ions and the magnetic superexchange interaction between Co^{4+} ion and another tetravalent transition metal ion at the octahedral site.

Electrical conductivity of perovskite type oxides, $SrCoO_{3-\delta}$ and $(La_{1-X}Sr_X)CoO_3$ were measured to discusse the behavior of 3d electrons of Co ions on the basis of the results of the magnetic and metallic properties. Mössbauer effect of ^{57}Fe doped in $SrCoO_3$ was examined to clear up the sign of magnetic hyperfine field of Fe^{4+} in ferromagnetic oxides.

These results are presented in this paper and general discussion was made.

Chapter 2 EXPERIMENTAL PROCEDURE

2-1) High oxygen pressure apparatus (29)

The schematic diagram of the high oxygen pressure apparatus is shown in Fig. 2. For safty, water was chosen as a pressure transmitting medium. Oxygen gas compressed by high pressure water was led into the reactor made of stellite No.25. For annealing under high oxygen pressures, sample was charged in a gold capsule with an open end and was placed in a reactor. After the reactor was filled with oxygen gas at a desired pressure at room temperature, it was heated by an electric furnace set outside.

Using this apparatus, the present experiment was performed under high oxygen pressures of 5-260 MPa at 523-673K for 24-170 hours.

2-2) X-ray diffraction

The products were identified by X-ray powder diffraction with filtered CuKα or CoKα radiations. Cell constants of products were recorded at a slow scan rate of 1/4 °/min using silicon powder as an internal standard material.

The isotropic temperature factor (B) of powdered samples was calculated as follows: The intensity of each reflection in the range of $20^\circ \leq 2\theta \leq 100^\circ$ was measured with Ni-filtered CuKα radiation. After appling Lorentz and polarization correction, the observed structure factor

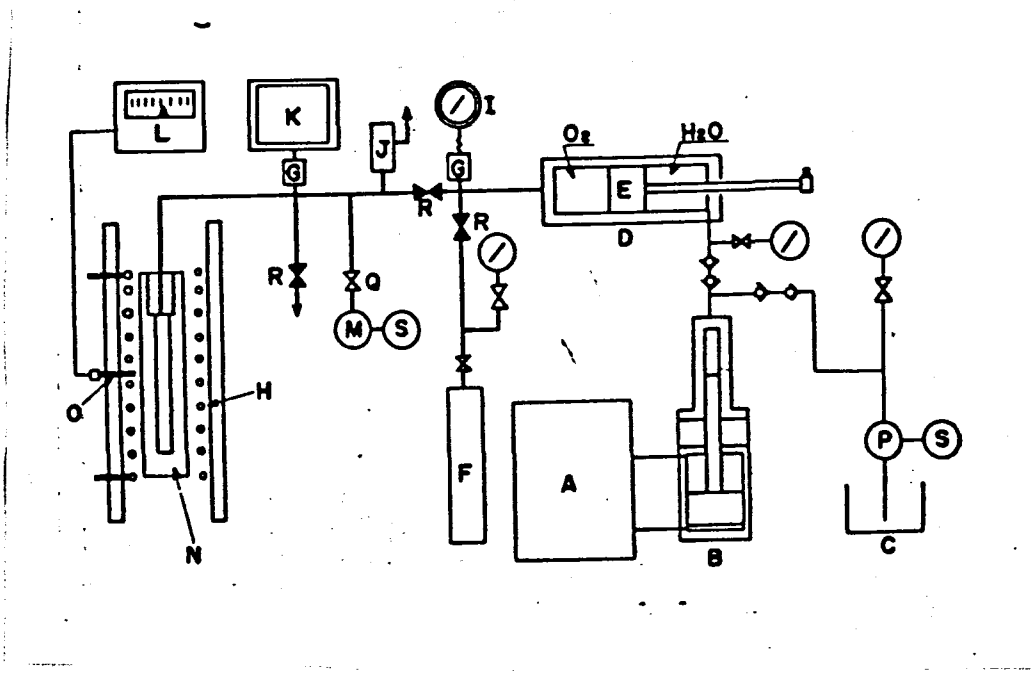

Fig. 2 Diagrammatic arrangements of high pressure apparatus.

A: oil pump unit, B: intensifier, C: water tank, D: oxygen gas compressor, E: piston, F: oxygen reservoir, G: pressure cell, H: furnace, I: pressure indicator, J: rupture cylinder, K: pressure recorder, L: temperature controller, M: vaccum pump, N: reactor, O: thermocouple, P: water pump, Q: stop valve, R: stop valve, S: electron motor

$|F_{obs.}|$ was calculated from the intensities. A least-square refinement was performed by "A Fortran IV Computer Program for Structure Factor Calculation and Least-Squares Refinement of Crystal Structure." system on the temperature factor (30).

2-3) Chemical analysis

The oxygen content in each sample was determined by chemical analysis (31). The total amount of cobalt (Co^{3+} and Co^{4+} ions) was determined as follows: The samples (about 0.2-0.5g) was dissolved in hydrochloric acid and α-nitroso-β-naphthol was added to this solution. The precipitation was filtered off and burnt in a crucible at 923-1023K. The cobalt content was weighed as Co_3O_4. The ratio Co^{3+}/Co^{4+} was determined by the oxidation-reduction (redox) method. After KI solution and hydrochloric acid were added to dissolve the sample (100-200mg) in a flask, the solution was titrated with a standard sodium thiosulfate solution (1/20N) using the soluble starch as an indicator.

2-4) Magnetic measurement

Magnetic susceptibility was measured using an automatic recording magnetic balance in the temperature range from 77 to 300K in a field of 8 kOe. The magnetic field was measured by the Gauss meter. The magnetic field gradient was calibrated relative to Mohr's salt ($FeSO_4(NH_4)$

$SO_4 6H_2O$). The temperature was measured with AuCo-Cu thermocouple. The thermocouple was located on the sample chamber made by Cu metal. The thermocouple was calibrated by using the values of the magnetic susceptibility of Mohr's salt at various temperatures. The Néel temperature (T_N) was determined from the maximum in the susceptibility curve. The paramagnetic Curie temperature (T_θ) and the mole Curie constant (Cm) were determined by the application of Curie-Weiss law in the paramagnetic region.

The value of saturation magnetization per gram (σ) calculated using Ni powder as a standard (σ_{Ni}= 54.39 emu/g at 288K) is given as follows,

$$\sigma = 54.39(w_{Ni}/w_s)(F_{Ni}/F_s) \qquad \text{--- (2)}$$

where w_{Ni} is the weight of Ni powder, w_s is the weight of sample, F_{Ni} is the force caused by the magnetic field for Ni and F_s is the force caused by the magnetic field for the sample. The spontenious magnetization at OK (σ_o) was determined from the σ-T curve.

The Curie temperature (Tc) was determined from the σ^2-T curve (32) and the magnetic moment per molecule ($\bar{n}$) was calculated using the following equation.

$$\bar{n} = (M \cdot \sigma_o)/(N \cdot \mu_B) \qquad (3)$$

where M is the mole weight of the sample, N is Avogadro number and μ_B is the Bohr magneton ($\mu_B = 9.28 \times 10^{-21}$, $N = 6.02 \times 10^{23}$). The blank tests from 77 to 300K were carried out before and after the measurements.

2-5) Electrical conductivity measurement

The powdered samples were compressed into a pellet form (15×5×5mm) under a pressure of about 100 MPa and then the pellets were sintered at 1273-1573K for 24 hours in a flow of pure oxygen gas. The oxygen-deficient samples obtained in this way were annealed under high oxygen pressures at 573K for 1 week. Electrical conductivity was measured by a standard four probes method in the temperature range from 77 to 300K.

2-6) Mössbauer effect measurement

Mössbauer effect measurement was carried out using a 1024 multichannel analyzer at liquid helium temperature and room temperature. The source (^{57}Co) was always kept at room temperature. For the calibration of velocity scale of absorption spectra, Fe metal was used as a standard absorption. A Westinghouse superconductor solenoid was used for the Mössbauer measurement in the present of an external field. The field direction was parallel with the incident gamma ray beam. The strength of the applied field was 45 kOe and the temperature of the sample was 4.2K.

Chapter 3 EXPERIMENTAL RESULTS

3-1) $SrCoO_{3-\delta}$ system

Powders of $SrCO_3$ and $CoCO_3$ were weighed in an equimole proportion and milled for 24 hours with aceton. After drying the mixed powders at 373K, the mixture was pre-fired in air at 1073K for 24 hours, then ground and fired at 1273K in a flow of pure oxygen gas for 24 hours. The product was indexed as a tetragonal perovskite type structure from the X-ray powder diffraction (19); a=0.3838 nm, c=0.3852 nm. The oxygen-deficient products obtained in this way were annealed under high oxygen pressures of 5-260 MPa at 523-673K for 24-72 hours (33).

The X-ray powder diffraction patterns of the annealed samples were completely indexed as the cubic perovskite structure. The oxygen deficiency (δ) in each product was determined by chemical analysis. Table 2 shows the values of δ in $SrCoO_{3-\delta}$ prepared under different annealing conditions. Cell constants were calculated from X-ray powder diffraction method. The relation between cell constants and Co^{4+} ion content is shown in Fig. 3. The cell constants decrease linearly with increasing Co^{4+} ion content. It is expected that the decrease of a-axis is caused by the difference of ionic radius between Co^{3+} and Co^{4+} ions at octahedral site. From the extrapolation of the present results, the cell constant of $SrCoO_3$ without oxygen deficiency

Table 2 δ values in $SrCoO_{3-\delta}$

Specimen number	Annealing Conditions: Temp. (K)	Annealing Conditions: Oxygen pressure (MPa)	Annealing Conditions: Time (hr)	Co^{4+}/Co (%)	δ
1	623	5	24	49	0.26
2	523	8	72	53	0.24
3	623	20	72	61	0.20
4	623	50	72	62	0.19
5	573	50	72	70	0.15
6	673	260	72	80	0.10
7	573	100	72	84	0.08
8	573	200	72	90	0.05

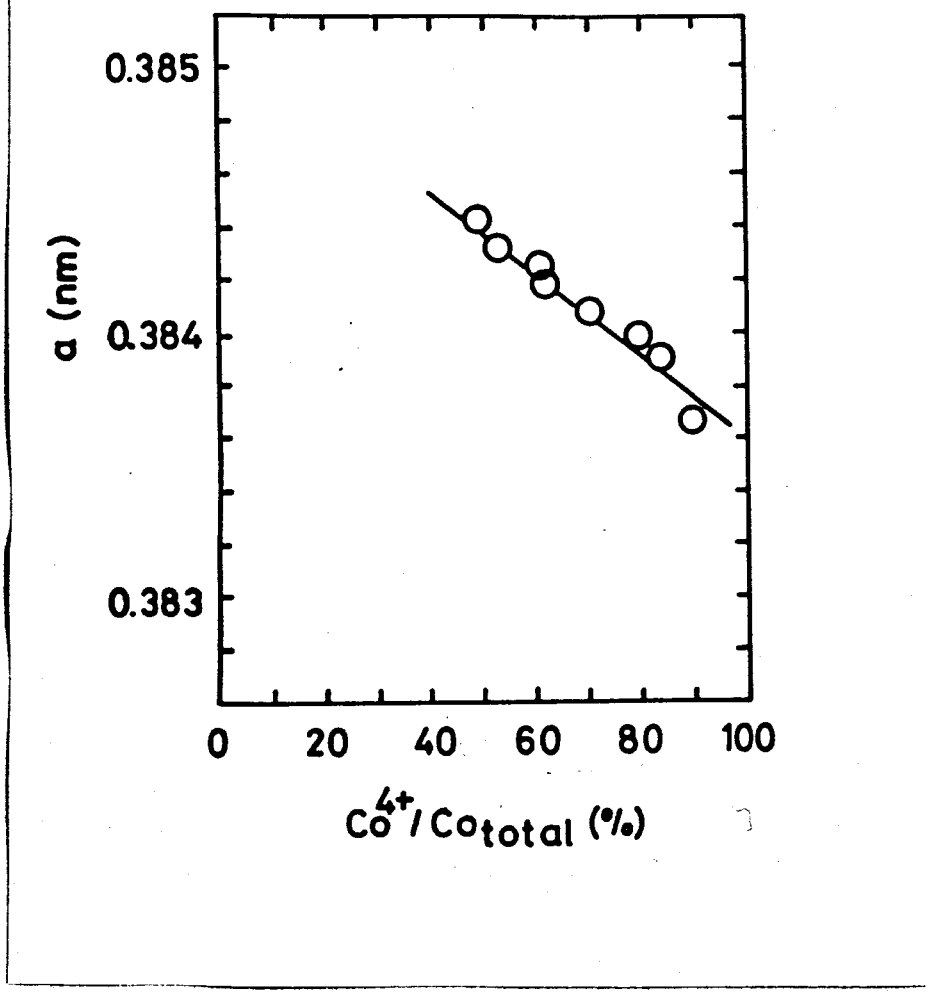

Fig. 3 Cell constant vs. Co^{4+} content in the system $SrCoO_{3-\delta}$.

was determined to be a=0.3836 nm as shown in Fig. 3.

Magnetic properties of all samples were measured by an automatic recording magnetic balance in the temperature range from 77 to 300K. It is known that $SrCoO_3$ is a ferromagnet with the Curie temperature of 200K (19), and $SrCoO_{2.5}$ whose structure is brownmillerite is an antiferromagnet with the Néel temperature of 570K (34). All samples of $SrCoO_{3-\delta}$ under the present investigation exhibited ferromagnetism below 215K. The spontenious magnetization (σ) per gram and the reciprocal susceptibility per gram ($1/\chi$)of $SrCoO_{2.85}$ as a function of the temperature are shown in Fig. 4. The Curie temperature (Tc) determined from the σ^2-T curve is shown as a function of Co^{4+} ion content in Fig. 5. Tc increases linearly with increasing Co^{4+} ion content. By extrapolation from the present results, Tc of $SrCoO_3$ without oxygen deficiency was estimated to be about 222K.

The values of spontenious magnetization at 0K (σ_0) of $SrCoO_{3-\delta}$ were estimated from the σ-T curves. σ_0 increases linearly with increasing Co^{4+} ion content and the value of σ_0 for $SrCoO_3$ is estimated to be 45.9 emu/g, which is relatively larger than that expected, assuming that the electron configuration of Co^{4+} ion is the low spin state with the $(d\varepsilon)^5(d\gamma)^0$. The magnetic moment ($\bar{n}$) at 0K was calculated from the values of σ_0 and is shown as a function of Co^{4+} ion content in Fig. 6. As well as

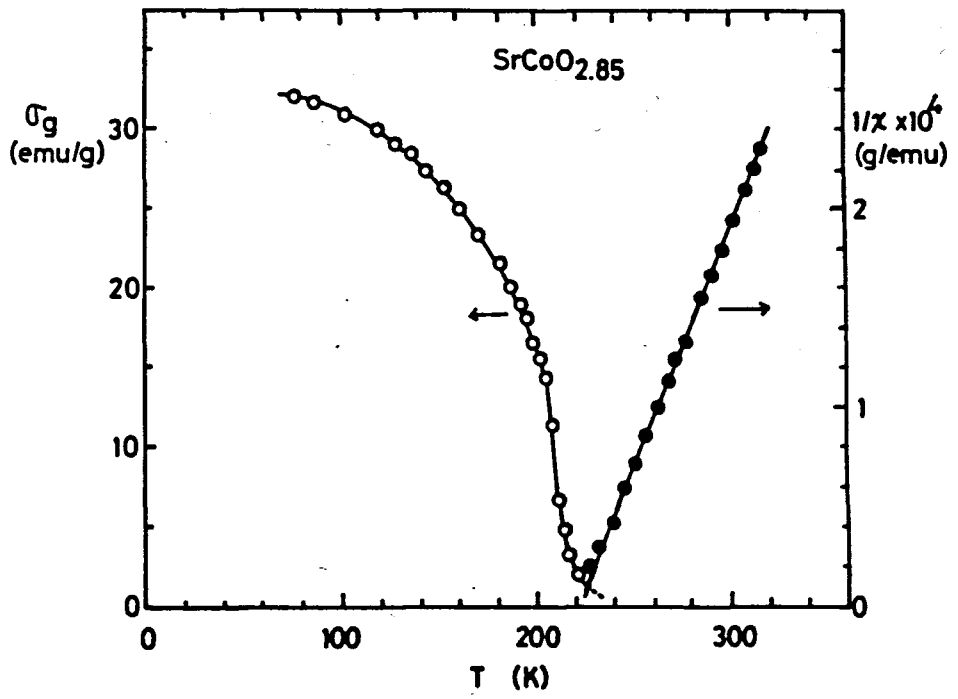

Fig. 4 Magnetic susceptibility vs. temperature and reciprocal susceptibility vs. temperature for $SrCoO_{2.85}$.

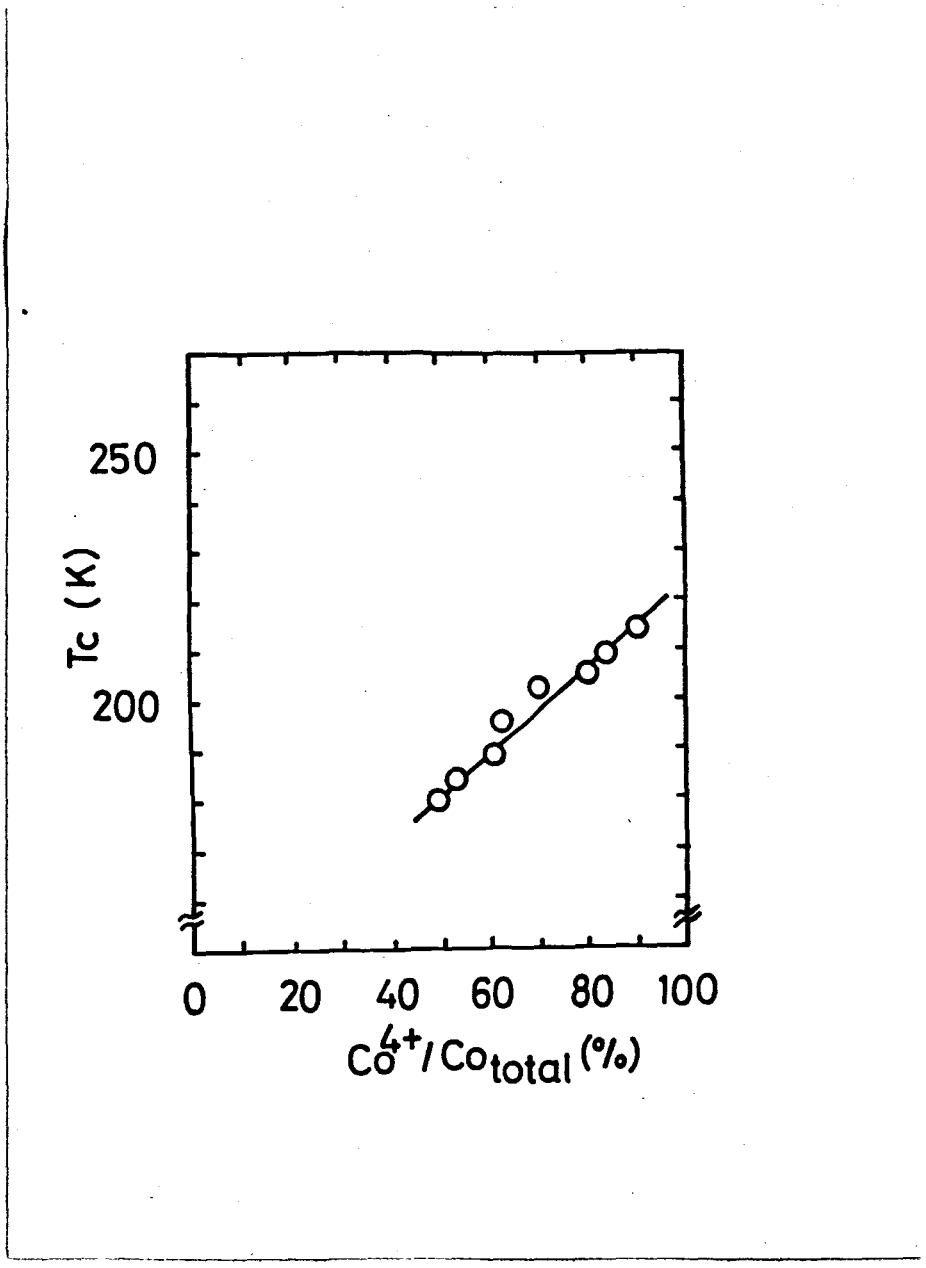

Fig. 5 Curie temperature vs. Co^{4+} content in the system $SrCoO_{3-\delta}$.

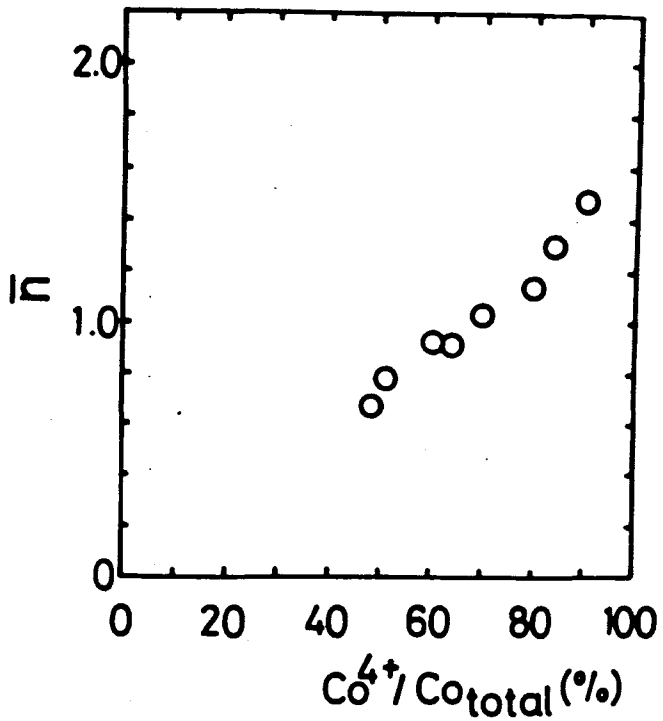

Fig. 6 Magnetic momenta vs. Co^{4+} content in the system $SrCoO_{3-\delta}$.

σ_o, $\bar{n}$ increases linearly with increasing Co^{4+} ion content and $\bar{n}$ for $SrCoO_3$ is estimated to be 1.60.

In the paramagnetic region, the relation between the reciprocal susceptibility ($1/\chi$) and the temperature (T) was linear. The effective magnetic moment was calculated from the linear portion of this curve according to the usual relation.

$$\mu_{eff} = 2.82\sqrt{\chi_m(T-T_\theta)} \qquad \cdots (4)$$

where μ_{eff} is the moment per molecule in Bohr magneton, χ_m is the molar susceptibility, T is the temperature in Kelvin and T_θ is the paramagnetic Curie temperature. The variation of T_θ and μ_{eff} are shown in Figs. 7 and 8 as a function of the Co^{4+} ion content. In Fig. 8, open circles indicate the observed values and a broken line is drawn for the theoretical values calculated under the following assumptions of the spin state of Co^{4+} and Co^{3+} ions. One is the high spin state of Co^{3+} ion with the $(d\varepsilon)^4(d\gamma)^2$ and the low spin state of Co^{4+} ion with the $(d\varepsilon)^5(d\gamma)^0$, and the other is the low spin state of Co^{3+} ion with the $(d\varepsilon)^6(d\gamma)^0$ and the low spin state of Co^{4+} ion with the $(d\varepsilon)^5(d\gamma)^0$. From these results, it is expected that the electron configuration of Co^{3+} and Co^{4+} ions are low spin state. As seen in Fig. 8, μ_{eff} for $SrCoO_3$ at Co^{4+}/Co_{total}=100 % is extrapolated to be approximately μ_{eff}=3.0.

The electrical conductivity of $SrCoO_{3-\delta}$ was measured

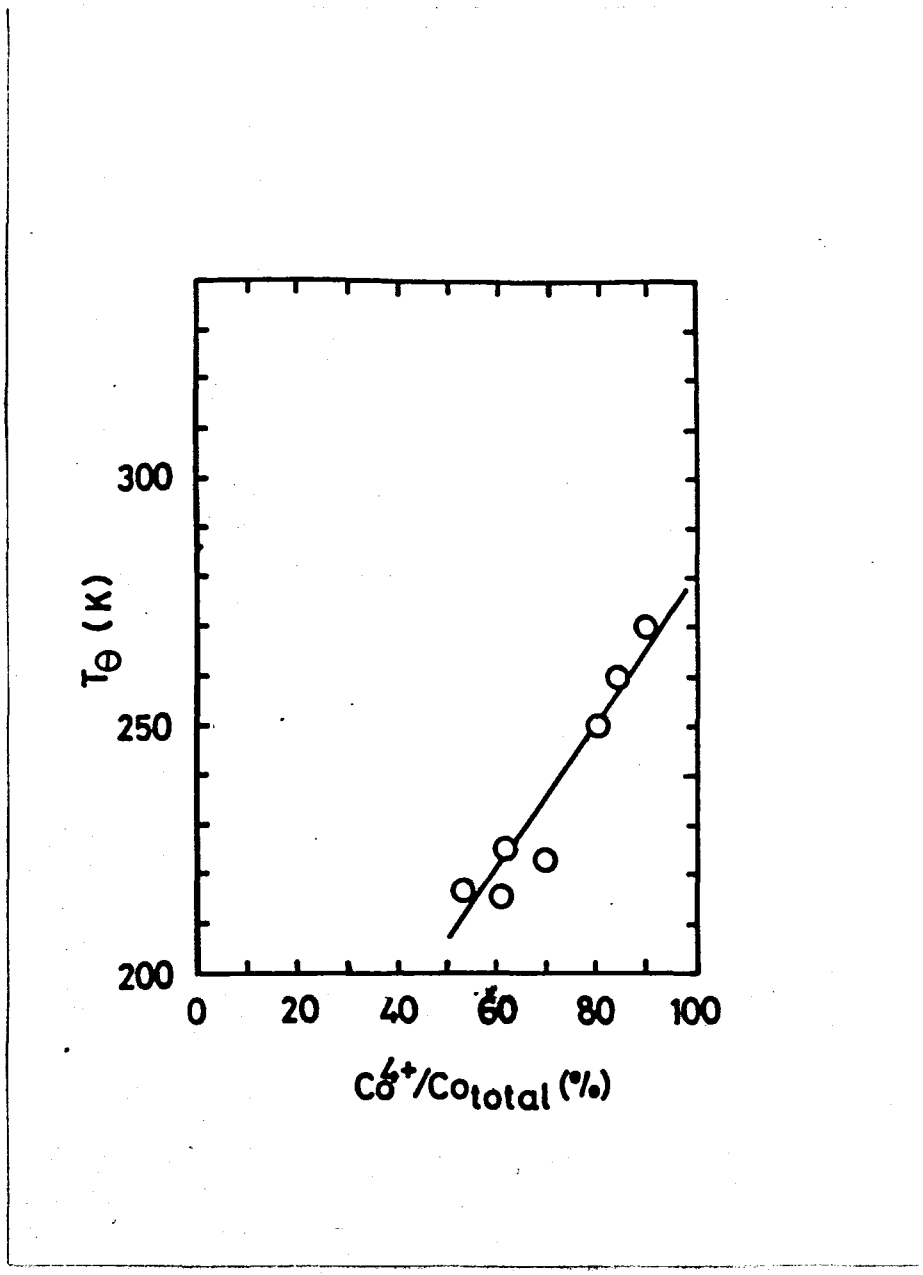

Fig. 7 Paramagnetic Curie temperature vs. Co^{4+} content in the system $SrCoO_{3-\delta}$.

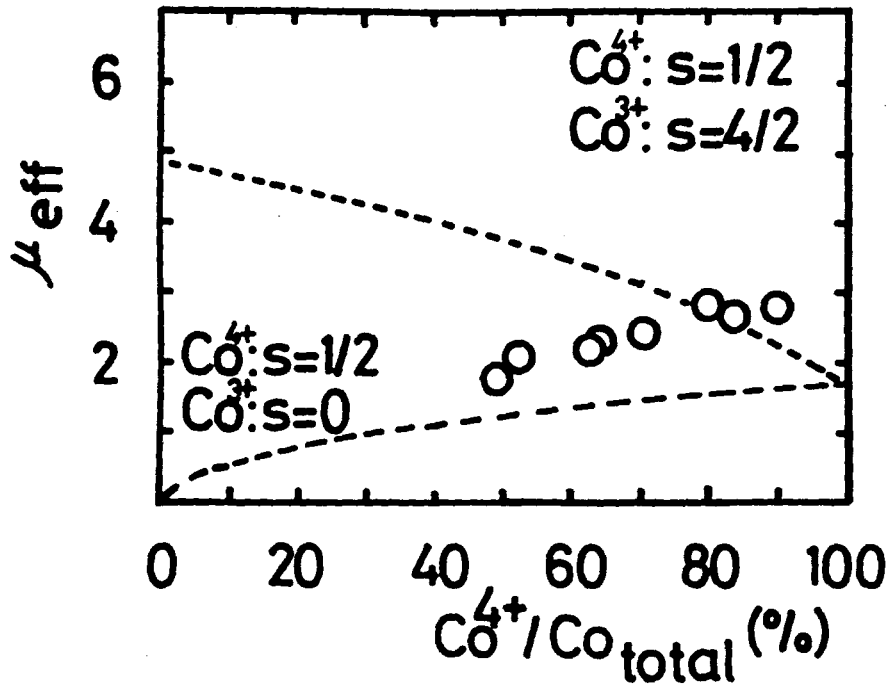

Fig. 8 Effective magnetic moment vs. Co^{4+} content in the system $SrCoO_{3-\delta}$.

in the temperature range from 77 to 300K (35).

X-ray powder diffraction patterns of all pellet samples under high oxygen pressures were completely indexed as the cubic perovskite structure. Table 3 shows the ratio of Co^{4+}/Co_{total} and the value of δ in $SrCoO_{3-\delta}$ prepared under different annealing conditions. Electrical resistivity data in the temperature range from 77 to 300K are shown in Fig. 9. All samples with different oxygen deficiencies of $SrCoO_{3-\delta}$ show metallic behavior. In Fig. 9, the arrows indicate the Curie temperature of each samples. It is found that the magnetic transitions are independent of the electrical conductivity in $SrCoO_{3-\delta}$. In Fig. 10, the values of $\log\rho$ at 80K and 300K are plotted against the Co^{4+} ion content. As seen in this figure, $\log\rho$ decreases monotonously with increasing the oxygen deficiency.

The Mössbauer spectra of $SrCoO_3$ dopped ^{57}Fe were measured at 300K and 4.2K (36). Both $Sr(Co_{0.99}{}^{57}Fe_{0.01})O_3$ and $Sr(Co_{0.5}{}^{57}Fe_{0.5})O_3$ were prepared as follows. Powders of $SrCO_3$, $CoCO_3$ and $^{57}Fe_2O_3$ were weighed in desired proportions and milled. They were pre-fired at 1073K for 24 hours, then ground and fired at 1273K in a flow of pure oxygen gas for 24 hours. The products were annealed under high oxygen pressure of 100 MPa at 573K for 72 hours.

Fig. 11 shows the Mössbauer spectra of $Sr(Co_{0.99}{}^{57}Fe_{0.01})O_3$.

Table 3 δ values in $SrCoO_{3-\delta}$

Specimen number	Annealing Conditions: Temp. (K)	Annealing Conditions: Oxygen pressure (MPa)	Annealing Conditions: Time (week)	Tc (K)	Co^{4+}/Co (%)	δ
1	573	130	1	218	92	0.04
2	573	60	1	212	86	0.07
3	573	30	1	198	70	0.15
4	573	10	1	170	40	0.30

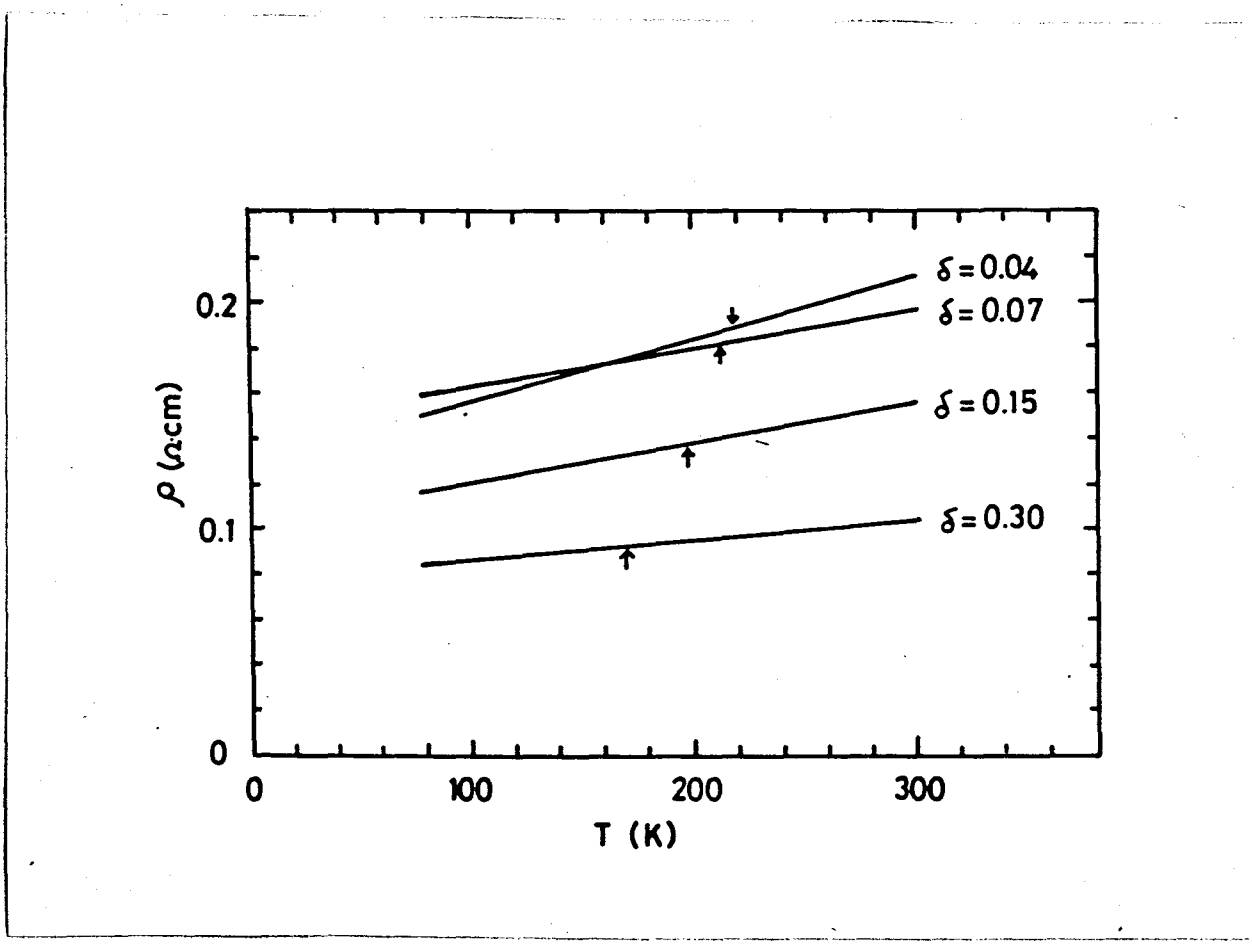

Fig. 9 Electrical resistivity vs. temperature in the system $SrCoO_{3-\delta}$.

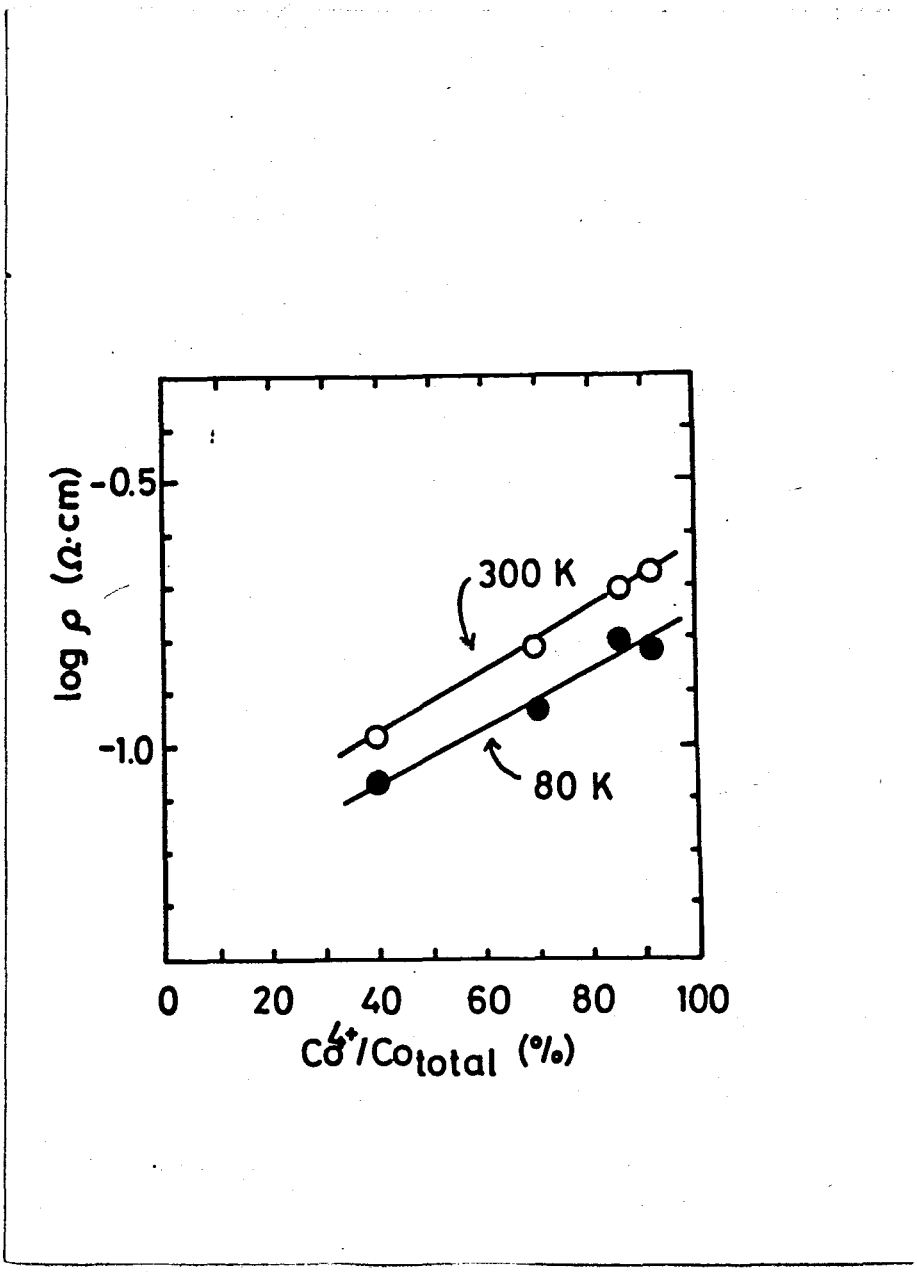

Fig. 10 Electrical resistivity vs. Co^{4+} content in the system $SrCoO_{3-\delta}$.

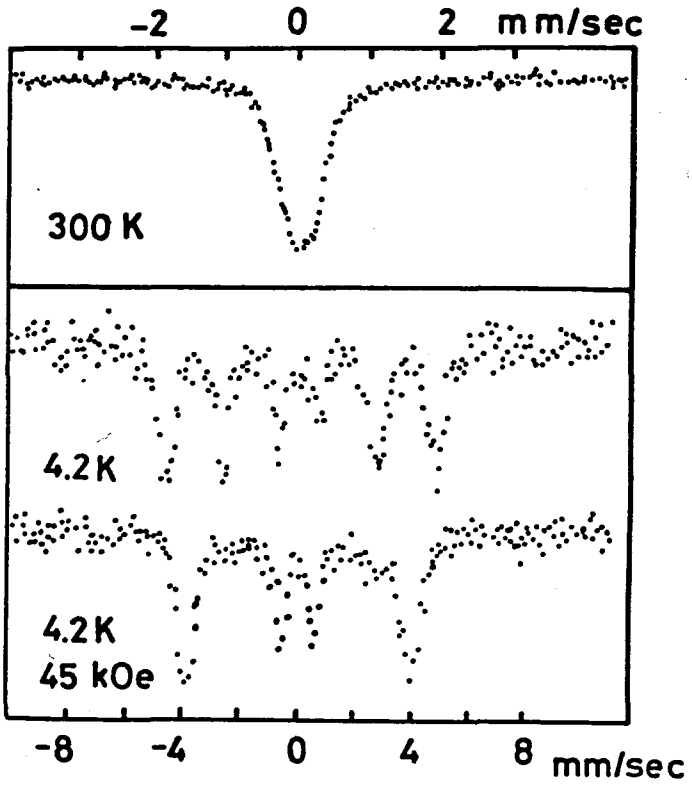

Fig. 11 Mössbauer spectra of $Sr(Co_{0.99}{}^{57}Fe_{0.01})O_3$ at 300K and 4.2K without external field and at 4.2K with an external field 45 kOe.

At 300K, the spectra is single absorption line whose isomershift is 0.05 mm/sec (vs. Fe) due to the typical Fe^{4+} state. The line width at half maximum is 0.67 mm/sec. At 4.2K, a magnetic hyperfine field of 296 kOe was observed. All Fe ions are confirmed to be a single Fe^{4+} state. When an external magnetic field (45 kOe) was applied in parallel to the gamma ray direction, No.2 and No.5 lines disappeared completely and the effective field was decreased.

Fig. 12 shows the Mössbauer spectra of $Sr(Co_{0.5}{}^{57}Fe_{0.5})O_3$. At 300K, the single absorption spectra certified the whole Fe atom being in a Fe^{4+} state. The isomershift is nearly $+0.05\pm0.02$ mm/sec. At 4.2K, a rather sharp six-line spectrum was observed and the hyperfine field was derived to be 302 kOe.

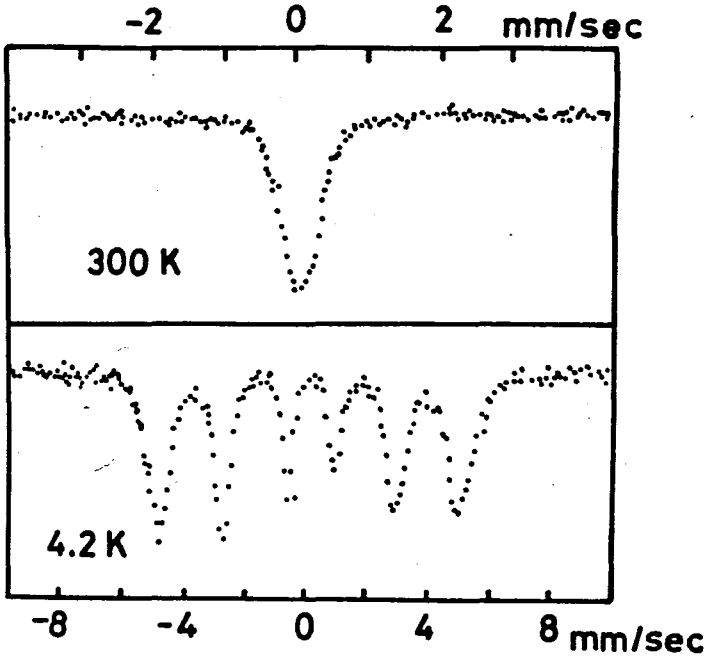

Fig. 12 Mössbauer spectra of $Sr(Co_{0.5}Mn_{0.5})O_3$ at 300K and 4.2K.

3-2) $(La_{1-X}Sr_X)CoO_3$ system $(0.5 \leqq X \leqq 1.0)$

Powders of La_2O_3, $SrCO_3$ and $CoCO_3$ were weighed in the desired proportions and milled for 24 hours with aceton. After drying the mixture at 373K, they were pre-fired in air at 1073K for 24 hours. The products obtained were reground and fired again for 24 hours at 1373-1573K in a flow of pure oxygen gas. The firing was repeated three times. The oxygen-deficient samples obtained in this way were annealed under the high oxygen pressure of 140 MPa at 573K for 72 hours (37).

X-ray powder diffraction patterns of all samples were completely indexed as the cubic perovskite structure. The relation between the composition and the cell constants is shown in Fig. 13. In the range of $0 \leqq X \leqq 0.5$, Askham et al. (26) found that $LaCoO_3$ showed a small rhombohedral distortion from the cubic form and had the cell constants of a=0.382 nm and $\alpha = 90^\circ 42'$. The distortion decreased with increasing Sr^{2+} ion contents and at about 50 % substitution of Sr^{2+} ion, $(La_{1-X}Sr_X)CoO_3$ was perfectly cubic with a=0.3832 nm.

Since those cobaltites containing higher Sr^{2+} ion contents have a tendency to involve the oxygen-deficiency as $(La_{1-X}Sr_X)CoO_{3-\delta}$, it is necessary to anneal them under high oxygen pressures to extinguish the oxygen vacancies. From the results of Section 3-1, the cell constant of $SrCoO_3$ was determined to be 0.3836 nm. By chemical analysis of Co^{4+} ion contents of these cobaltites, it was found

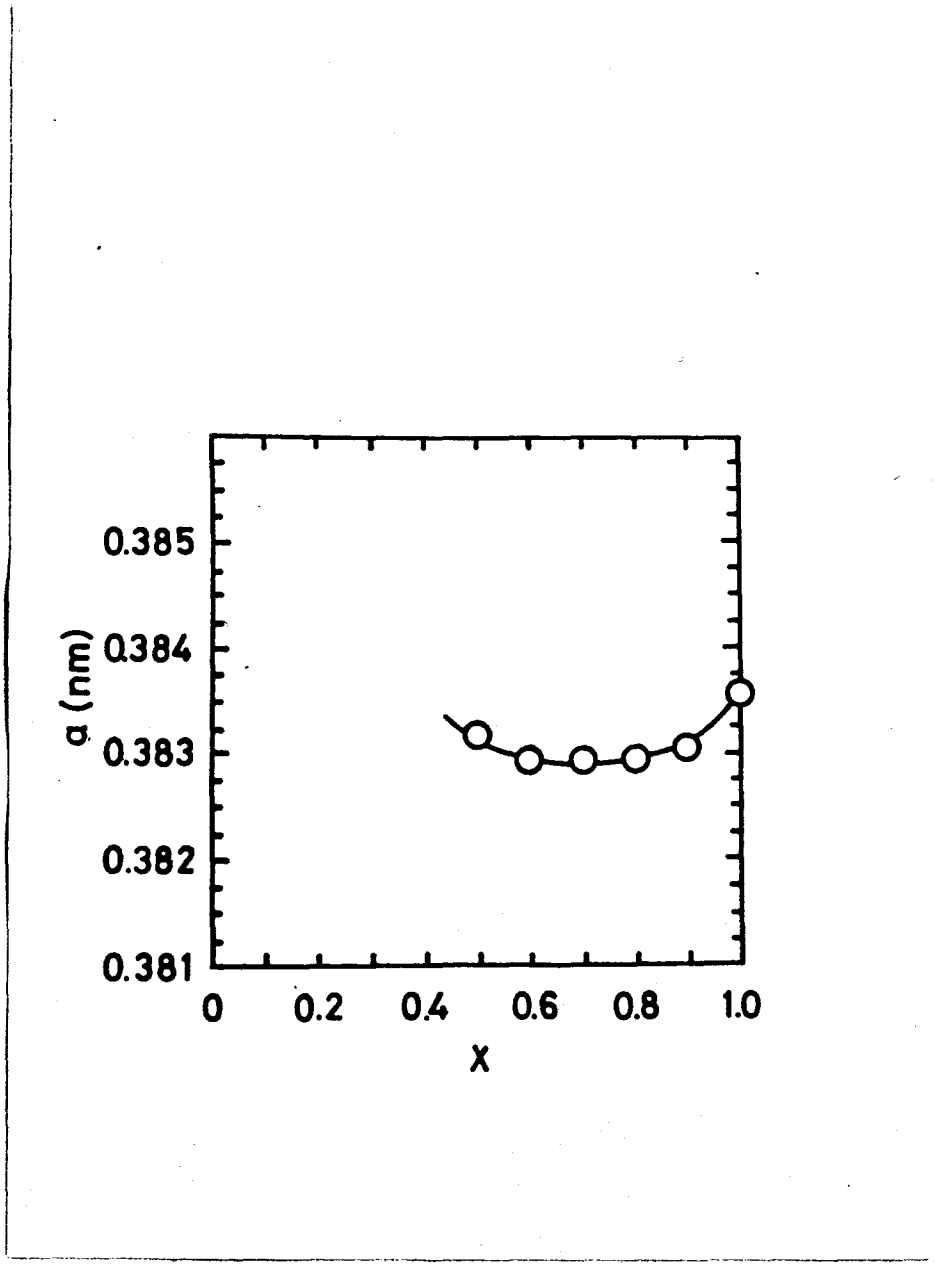

Fig. 13 Cell constant vs. composition in the system $(La_{1-X}Sr_X)CoO_3$.

that the sample of X=0.9 annealed under high oxygen pressures had an oxygen-deficiency and the cell constant of the sample without oxygen-deficiency was also determined by the same method adopted in the case of $SrCoO_3$. In the range of $0.5 \leqq X \leqq 0.8$, however, the oxygen-deficiency was not recongnized for all samples by means of the chemical analysis. The cell constants decreased monotonously with decreasing X from 1.0 to 0.7, and then increased linearly with decreasing X as shown in Fig. 13.

In the system $(La_{1-X}Sr_X)CoO_3$, it was found that these cobaltites exhibit ferromagnetism in the range of $0.05 \leqq X \leqq 0.5$ (24) and X=1.0. From the result of Section 3-1, the Curie temperature (Tc) and the paramagnetic Curie temperature (T_θ) of $SrCoO_3$ were 222K and 280K respectively. In the range of $0.5 \leqq X \leqq 1.0$, all cobaltites exhibited ferromagnetism below 300K and Tc determined from the σ^2-T curves is shown in Fig. 14 as a function of X. Tc increases monotonously with increasing X and reaches a maximum value of 280K at X=0.7, and then decreases linearly with increasing X in the range of $0.8 \leqq X \leqq 1.0$. The spontenious magnetization (σ) per gram and the reciprocal susceptibility per gram ($1/\chi$) of $(La_{0.3}Sr_{0.7})CoO_3$ as a function of temperature (T) in cobaltites are shown in Fig. 15. The values of the spontenious magnetization at 0K (σ_0) were estimated from the σ-T curve and are shown in Fig. 16 as a function of X. σ_0 shows the same tendency for Tc, and

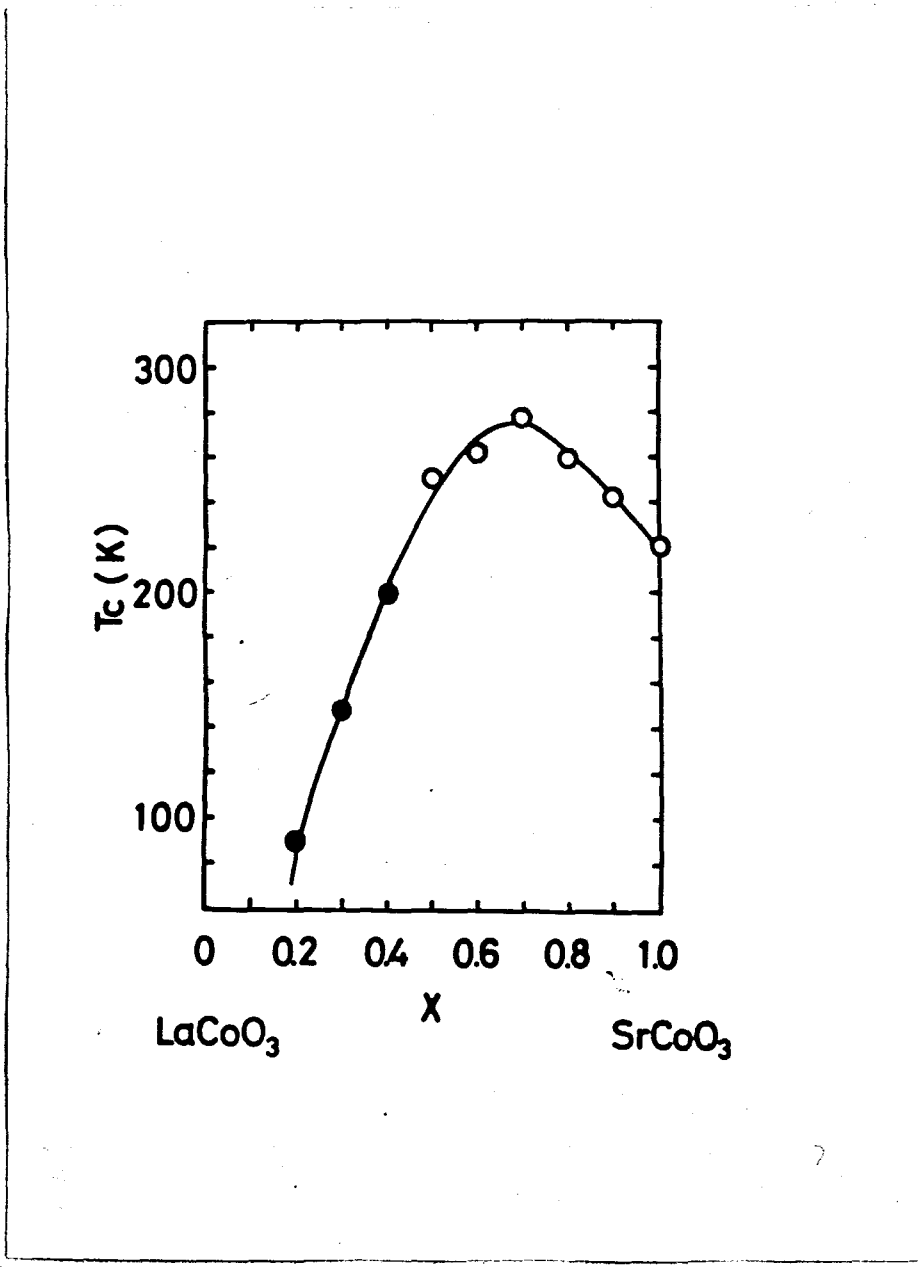

Fig. 14 Curie temperature vs. composition in the system $(La_{1-X}Sr_X)CoO_3$.

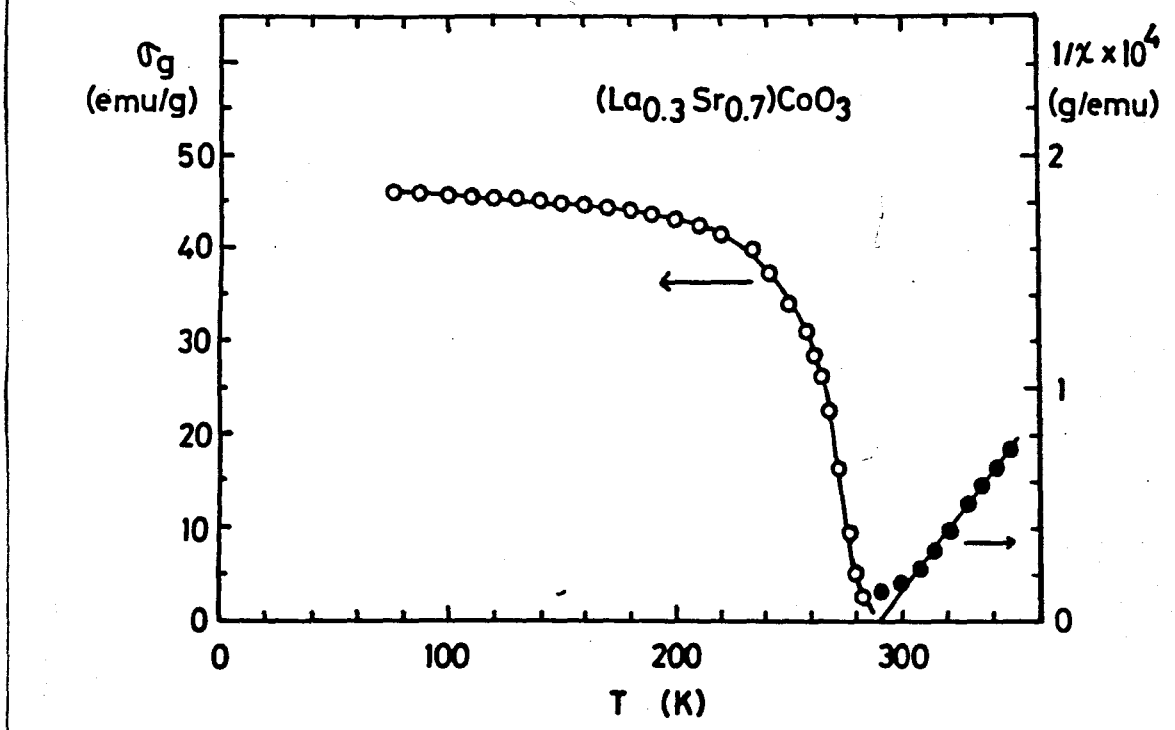

Fig. 15 Magnetic susceptibility vs. temperature and reciprocal susceptibility vs. temperature for $(La_{0.3}Sr_{0.7})CoO_3$.

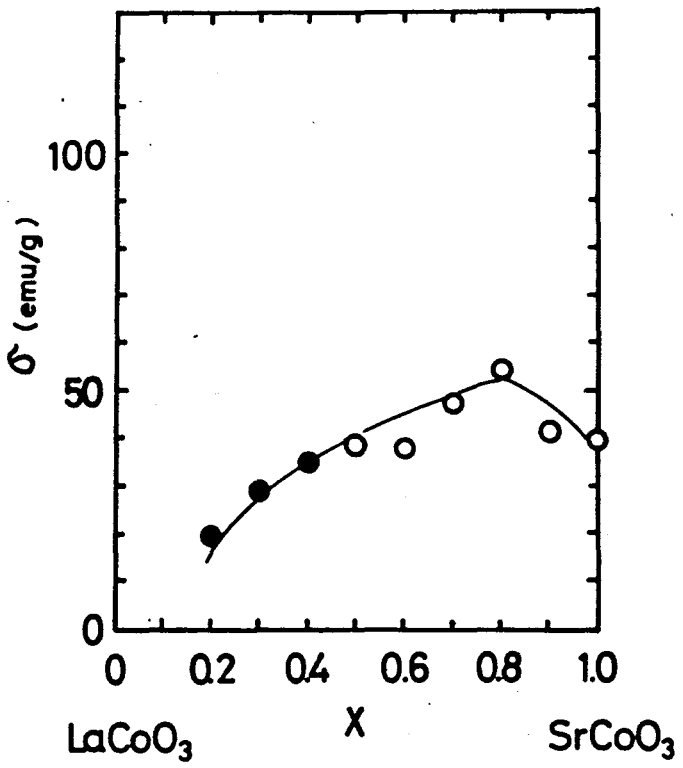

Fig. 16 Spontenious magnetization vs. composition in the system $(La_{1-X}Sr_X)CoO_3$.

σ_0 reaches the maximum value of 55 emu/g at X=0.8. The paramagnetic Curie temperature (T_θ) is shown in Fig. 17 as a function of X. In Figs. 14, 16 and 17, open circules indicate the observed values in the present investigation and the filled circules indicate the values reported by Raccah and Goodenough (24).

The temperature dependence of the paramagnetic susceptibility of cobaltites was determined in the paramagnetic region. The curve $1/\chi$ vs. temperature (T) was linear. The values of effective magnetic moment (μ_{eff}) calculated from the linear portion of the curve are shown in Fig. 18 as a function of X. Open circules indicate the observed values and the filled circules indicate the values reported by Jonker (22). The broken lines are drawn for the theoretical values calculated in each case of the following spin states of Co^{4+} and Co^{3+} ions located at the octahedral site; the high spin state of Co^{3+} ion with the $(d\varepsilon)^4(d\gamma)^2$ and the low spin state of Co^{4+} ion with the $(d\varepsilon)^5(d\gamma)^0$, the low spin state of Co^{3+} ion with the $(d\varepsilon)^6(d\gamma)^0$ and the low spin state of Co^{4+} ion with the $(d\varepsilon)^5(d\gamma)^0$, the high spin state of Co^{3+} ion with the $(d\varepsilon)^4(d\gamma)^2$ and the high spin state of Co^{4+} ion with the $(d\varepsilon)^3(d\gamma)^2$, and the low spin state of Co^{3+} ion with the $(d\varepsilon)^6(d\gamma)^0$ and the high spin state of Co^{4+} ion with the $(d\varepsilon)^3(d\gamma)^2$. As seen in Fig. 18, it is assumed that Co^{3+} ion is in the high spin state and Co^{4+} ion is

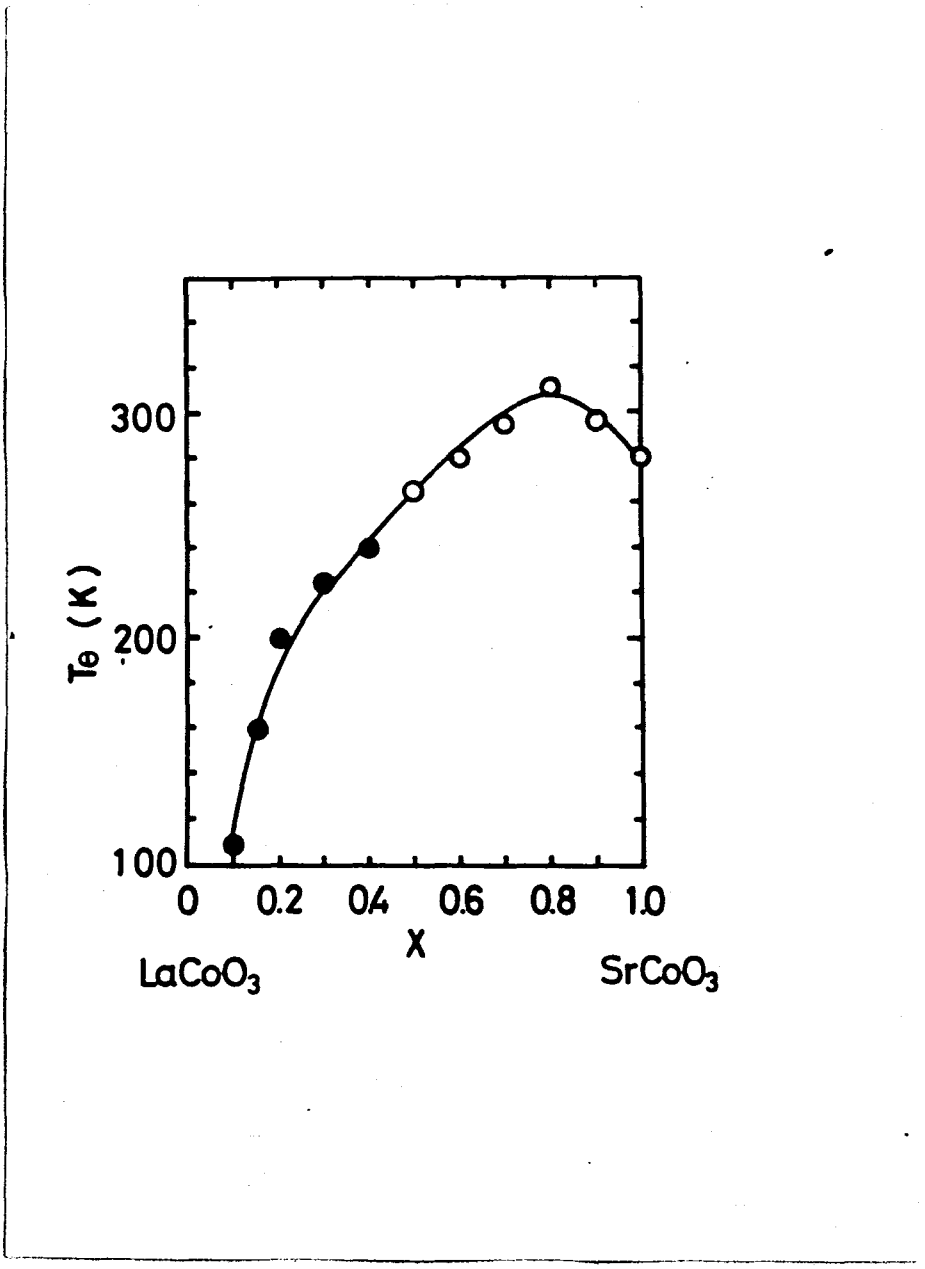

Fig. 17 Paramagnetic Curie temperature vs. composition in the system $(La_{1-X}Sr_X)CoO_3$.

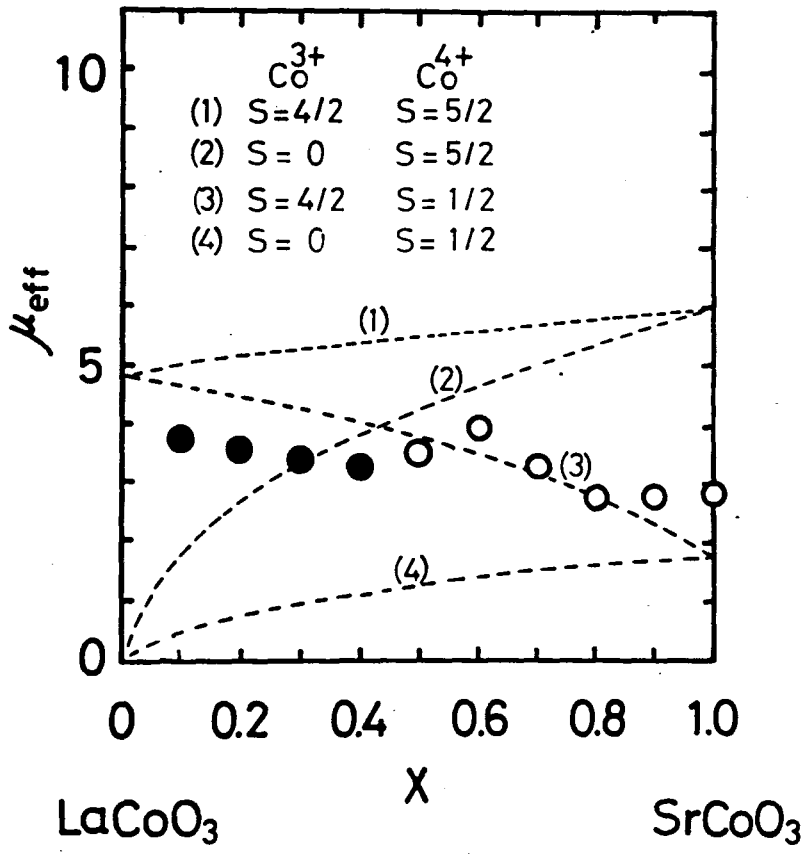

Fig. 18 Effective magnetic moment vs. composition in the system $(La_{1-X}Sr_X)CoO_3$.

the low spin state.

The electrical conductivity of $(La_{1-X}Sr_X)CoO_3$ was measured in the temperature range from 77 to 300K. The phases of the pellet samples were identified by X-ray powder diffraction with the filtered CoKα radiation. The electrical conductivity were measured by the standard four probes method (38).

X-ray powder diffraction patterns of all pellet form samples were completely indexed as the cubic perovskite structure, and the cell constants agreed with those of powdered samples of $(La_{1-X}Sr_X)CoO_3$ as shown in Fig. 13. The Curie temperature (Tc) of the pellet form samples were measured and agreed with the data of the powdered samples. The electrical resistivity data in the temperature range from 77 to 300K are shown in Fig. 19. All samples are good conductors and have metallic temperature coefficient. In Fig. 19, the arrows are the Curie temperature (Tc) of each sample. It is found that the magnetic transition is independent of the electrical conductivities in $(La_{1-X}Sr_X)CoO_3$. In Fig. 20, the values of $\log\rho$ at 80K and 290K were plotted against X. As seen in this figure, $\log\rho$ monotonously increases with increasing X. Since the samples annealed under high oxygen pressures have a little porosity, the measured values of electrical resistivity of samples are still higher.

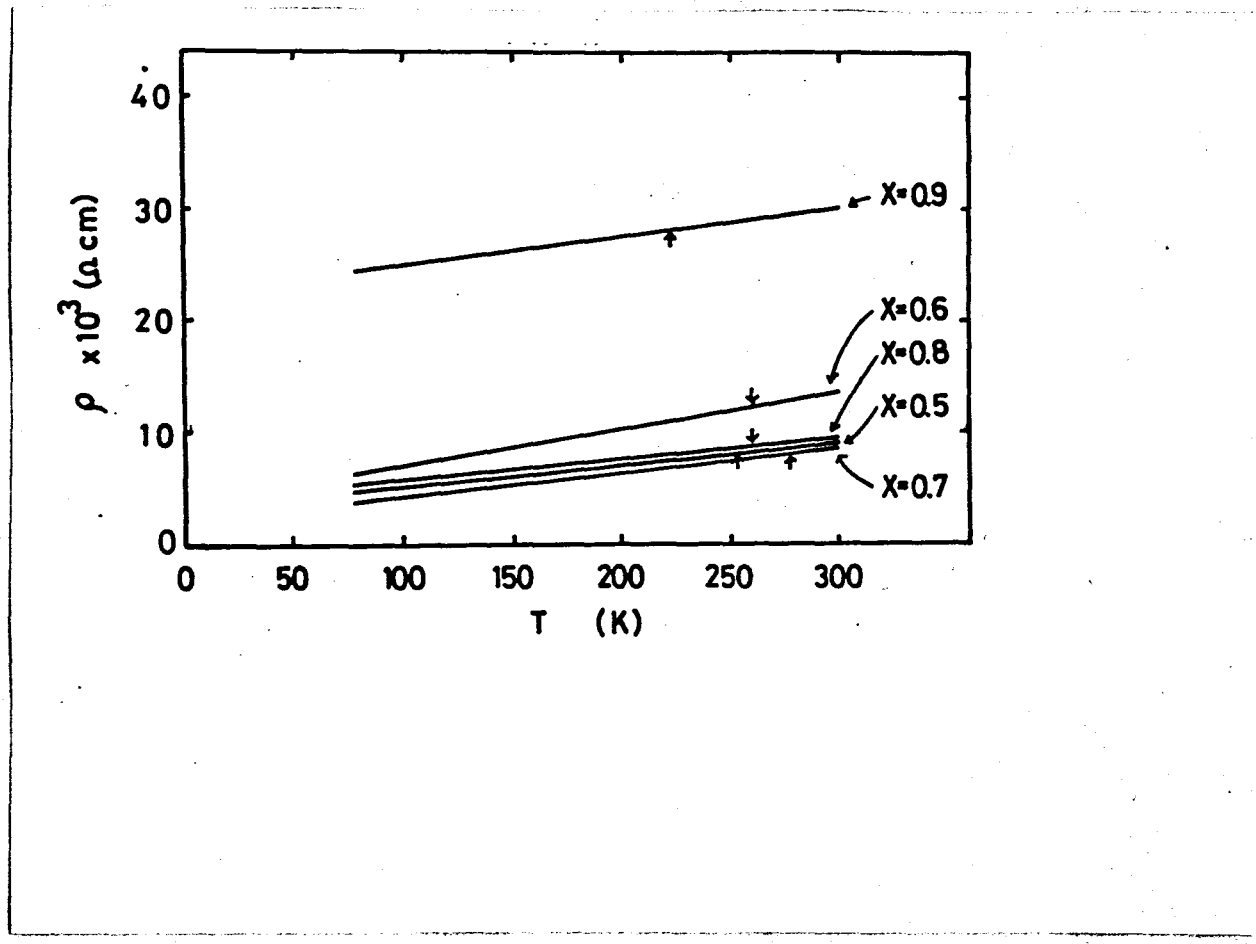

Fig. 19 Electrical resistivity vs. temperature in the system $(La_{1-X}Sr_X)CoO_3$.

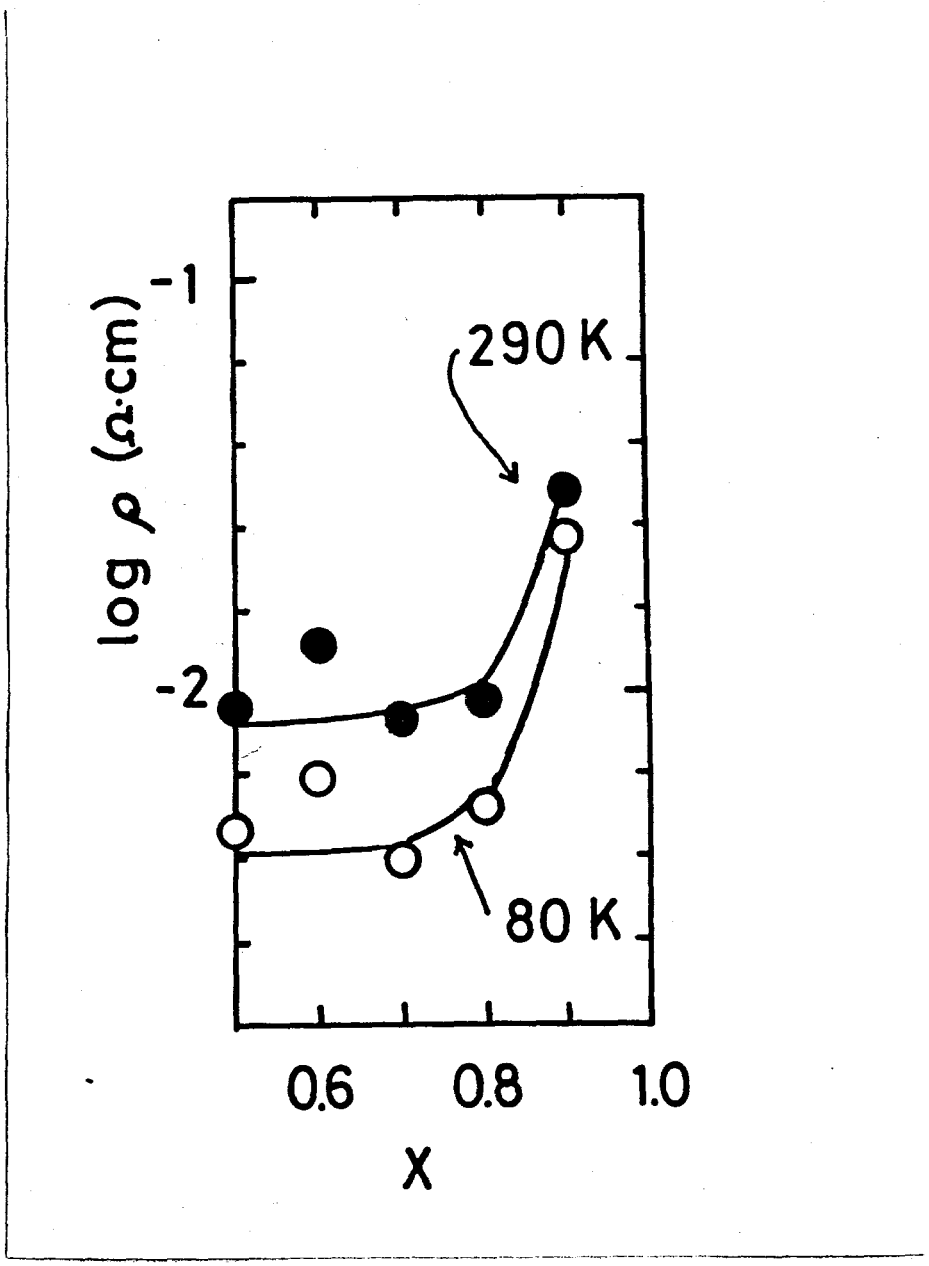

Fig. 20 Electrical resistivity vs. composition in the system $(La_{1-X}Sr_X)CoO_3$.

3-3) $Sr(Co_{1-X}Mn_X)O_3$ system

Powders of $SrCO_3$, $CoCO_3$ and $MnCO_3$ were weighed in the desired proportions and milled for 24 hours with aceton. After drying the mixtures at 373K, they were pre-fired in air at 1073K for 24 hours. The products obtained in the range of $0 \leqq X \leqq 0.5$ were ground and then fired at 1273-1623K in a flow of pure oxygen gas for 24 hours. The products obtained in the range of $0.6 \leqq X \leqq 1.0$ were fired at 1623K in a flow of argon gas for 24 hours. The firing was repeated three times. The oxygen-deficient samples obtained in this way were annealed under the high oxygen pressures of 140 MPa at 573K for 24 hours (39).

X-ray powder diffraction patterns of all samples were completely indexed as a cubic perovskite structure. The relation between the cell constants and the composition (X) is shown in Fig. 21. The cell constant linearly increased with increasing X in the range of $0 \leqq X \leqq 0.3$, and it decreased monotonously with increasing X in the range of $0.3 \leqq X \leqq 1.0$. From this result, it was understood that the distance of 0.1904 nm for Mn^{4+}-O was shorter than that of 0.1918 nm for Co^{4+}-O.

Magnetic properties were measured in the temperature range from 77 to 300K. In $Sr(Co_{1-X}Mn_X)O_3$ system, it is known that $SrCoO_3$ is a ferromagnet with the Curie temperature (Tc) of 222K and $SrMnO_3$ is an antiferromagnet with the Néel temperature (T_N) of 260K (15,40). In the range of

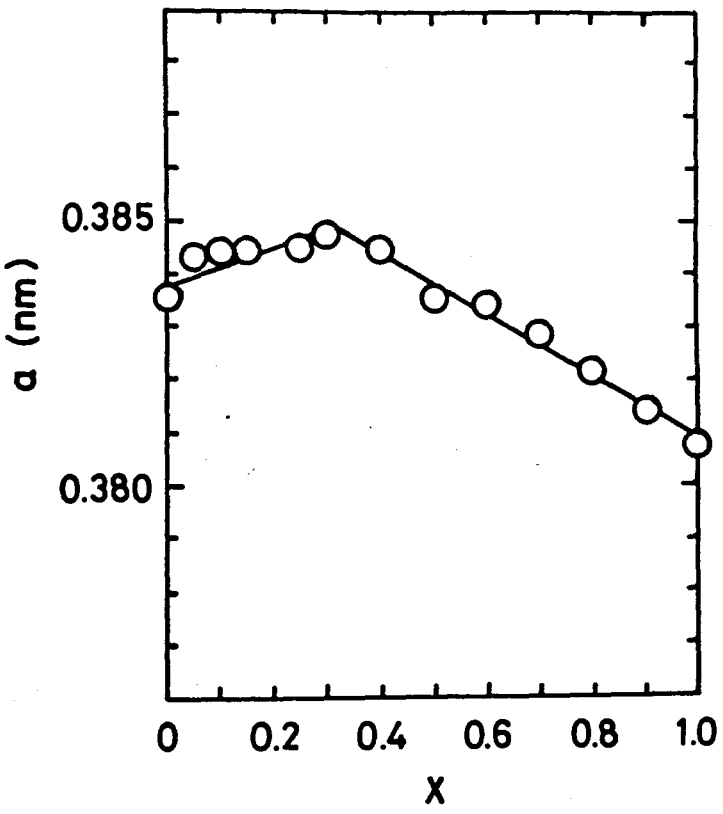

Fig. 21 Cell constant vs. composition in the system $Sr(Co_{1-X}Mn_X)O_3$.

$0 \leqq X \leqq 0.3$, the samples exhibited ferromagnetism whose paramagnetic Curie temperature (T_θ) was nearly equal to Tc, and in the range of $0.3 \leqq X \leqq 1.0$, the samples exhibited antiferromagnetism whose T_θ were below 0K. In Fig. 22, Tc determined from the σ^2-T curve and T_N determined from the maximum of χ-T curve are shown as a function of X. Tc decreased linearly with increasing X in the range of $0 \leqq X \leqq 0.3$ and T_N increased monotonously with increasing X in the range of $0.3 \leqq X \leqq 1.0$. The spontaneous magnetization (σ) per gram as a function of temperature (T) of ferromagnetic $Sr(Co_{1-X}Mn_X)O_3$ are shown in Fig. 23. The temperature dependence of the molar susceptibility of antiferromagnetic $Sr(Co_{1-X}Mn_X)O_3$ is also shown in Fig. 24. The values of the spontaneous magnetization at 0K (σ_o) were estimated from the σ-T curve in the range of $0 \leqq X \leqq 0.3$. σ_o decreased monotonously with increasing X, and Tc and σ_o for $Sr(Co_{0.9}Mn_{0.1})O_3$ were about 140K and 27.1 emu/g respectively. In Fig. 25, the paramagnetic Curie temperature (T_θ) was shown as a function of X in $Sr(Co_{1-X}Mn_X)O_3$. In the range of $0 \leqq X \leqq 0.3$, T_θ decreased monotonously with increasing X. In the range of $0.3 \leqq X \leqq 1.0$, T_θ was below 0K.

The temperature dependence of paramagnetic susceptibility of $Sr(Co_{1-X}Mn_X)O_3$ was determined in the paramagnetic region. The effective magnetic moment (μ_{eff}) calculated from the linear portion of the $1/\chi$-T curve

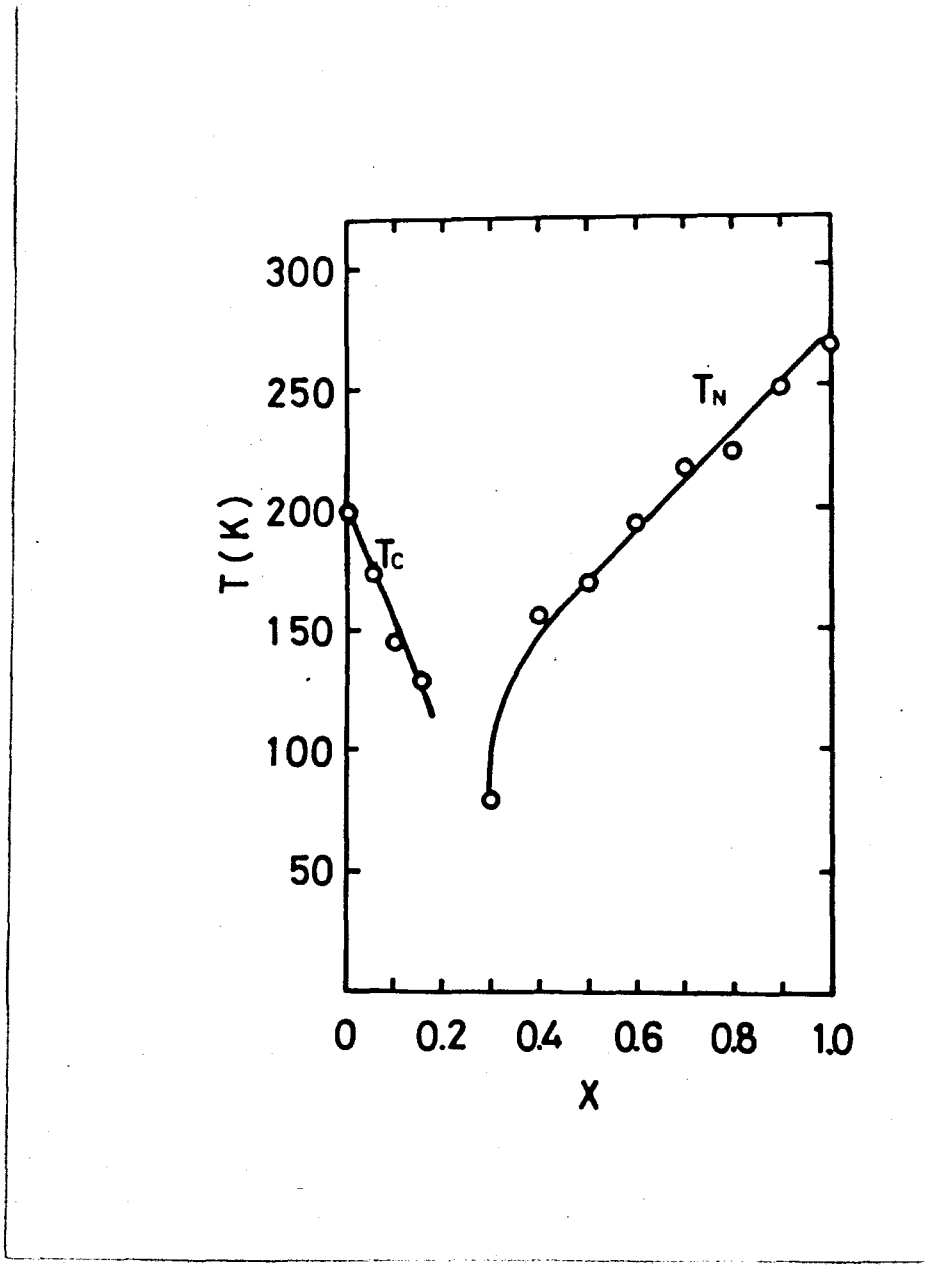

Fig. 22 Curie temperature and Néel temperature vs. composition in the system $Sr(Co_{1-X}Mn_X)O_3$.

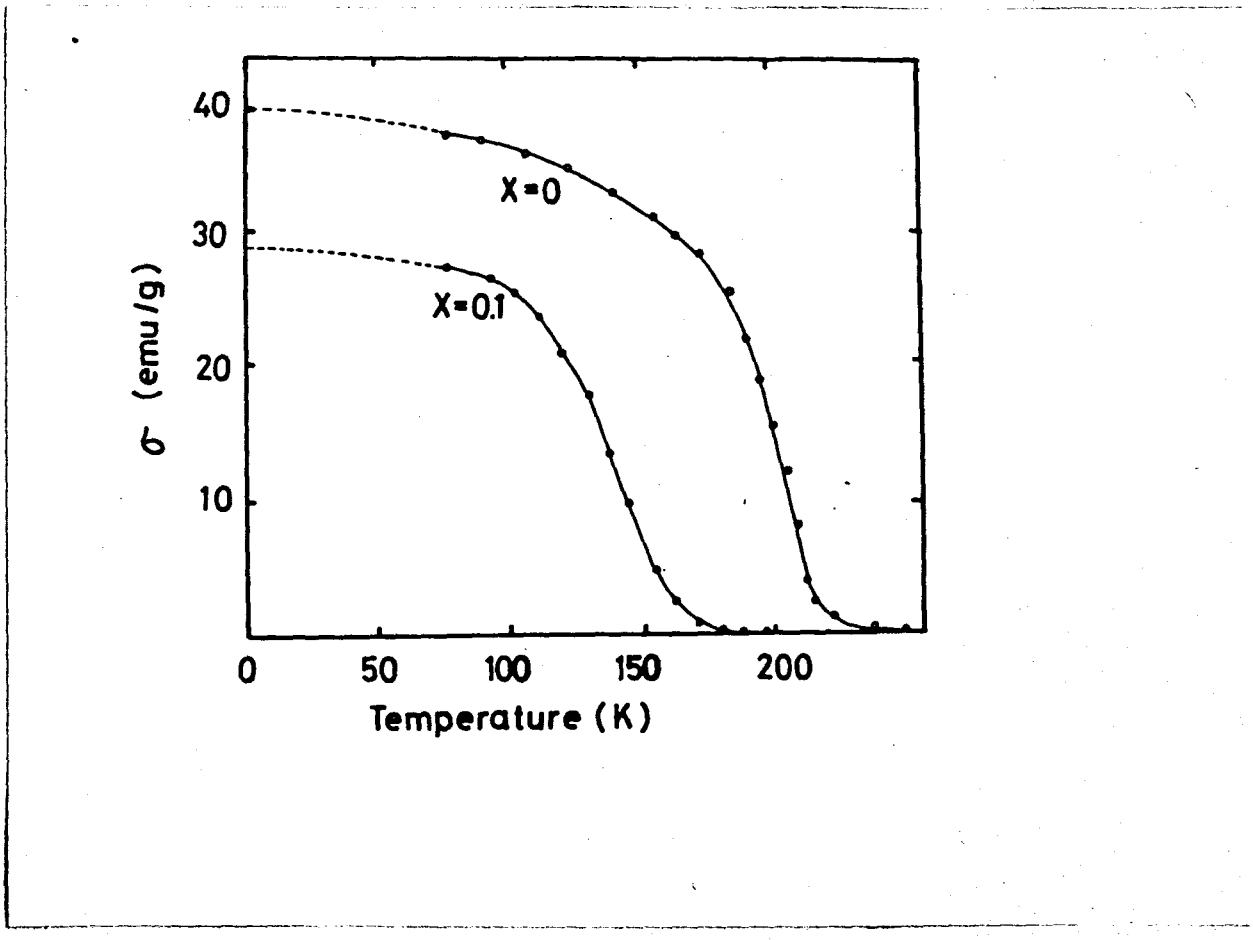

Fig. 23 Spontenious magnetization vs. temperature in the system $Sr(Co_{1-X}Mn_X)O_3$.

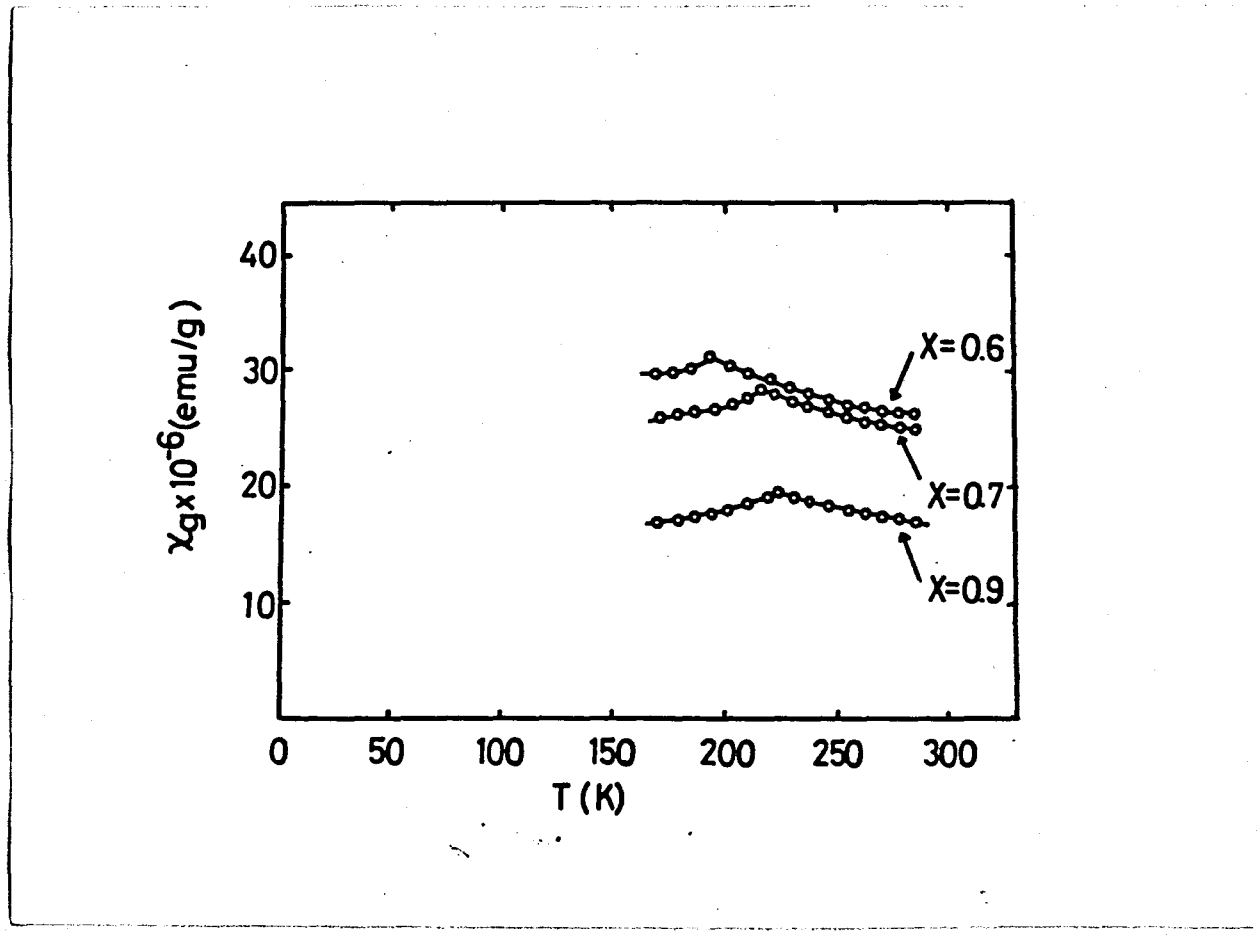

Fig. 24 Magnetic susceptibility vs. temperature in the system $Sr(Co_{1-X}Mn_X)O_3$.

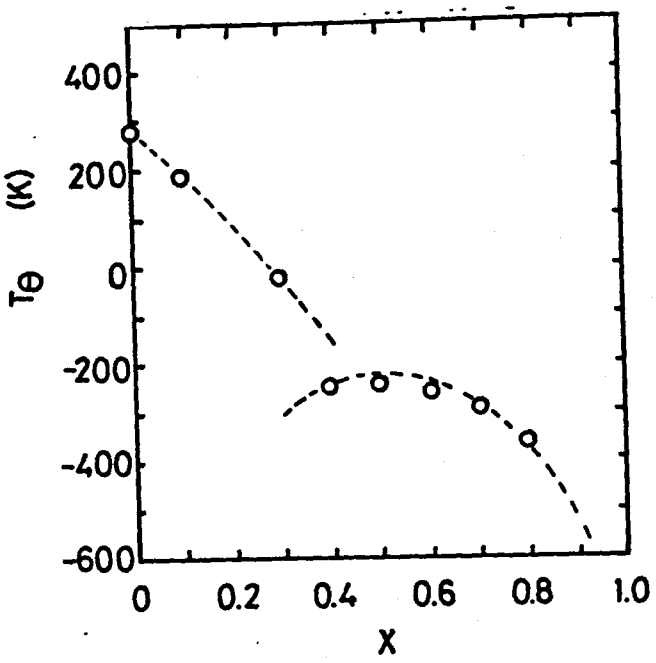

Fig. 25 Paramagnetic Curie temperature vs. composition in the system $Sr(Co_{1-X}Mn_X)O_3$.

is shown in Fig. 26 as a function of X. In this figure, circules indicated the observed values and the broken lines were drawn for the theoretical values calculated in the case of the following spin states of Co^{4+} and Mn^{4+} ions located at octahedral site; one is the high spin state of Co^{4+} ion with the $(d\varepsilon)^3(d\gamma)^2$ and the other is the low spin state of Co^{4+} ion with the $(d\varepsilon)^5(d\gamma)^0$. The Mn^{4+} ion with a $3d^3$ electron configuration has one spin state with the $(d\varepsilon)^3(d\gamma)^0$. Observed and calculated values of μ_{eff} were nearly equal to each other under the assumption of S=1/2 for Co^{4+} ion and S=3/2 for Mn^{4+} ion in the range of $0 \leqq X < 0.3$, and S=5/2 for Co^{4+} ion and S=3/2 for Mn^{4+} ion in the range of $0.3 \leqq X \leqq 1.0$.

To calculate the isotropic temperature factor of powdered samples, the intensity of each reflection was measured with Ni-filtered CuKα radiation in the range of $20^\circ \leqq 2\theta \leqq 100^\circ$. After the correction for background, absorption and extinction, the observed structure factor $|F_{ob}|$ was calculated under the assumption that strontium, cobalt, manganese and oxygen atoms occupied the special position of 1a, 1b, 1b and 3c respectively in the space group of Pm3m. A least square refinement was made with "A Fortrant IV Computer for Structure Factor Calculation and Least-Square Refinement of Crystal Structure." program (30) on temperature factor. In the refinement program, neutral atomic form factors were taken from International

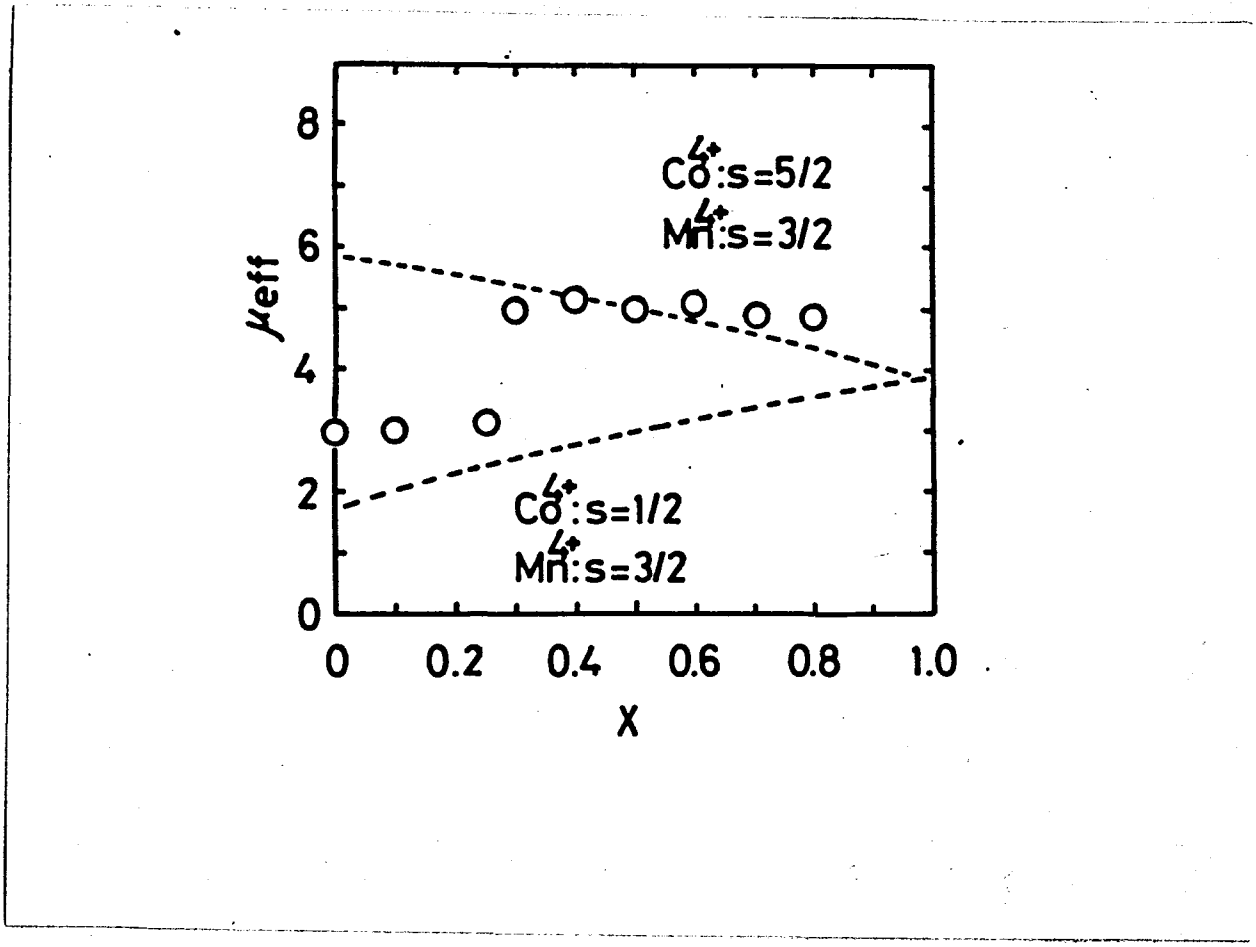

Fig. 26 Effective magnetic moment vs. composition in the system $Sr(Co_{1-X}Mn_X)O_3$.

Table for X-ray Crystallography (1962) (41).

The isotropic temperature factor calculated using the space group Pm3m is as follows; Sr: 2.38, Co: 4.25 and O: 7.94 for X=0 (R=5.7 %) and Sr: 1.97, Mn: 4.47 and O: 7.60 for X=1.0 (R=5.8 %). From these results, the isotropic temperature factor of strontium is ca. 2.00 and those of cobalt and manganese are ca. 4.00. To compare the isotropic temperature factor of oxygen for all samples, the isotropic temperature factors of strontium, cobalt and manganese were fixed as 2.00, 4.00 and 4.00 respectively. And the least square refinement on oxygen was performed for X=0, 0.1, 0.5, 0.8 and 1.0. The isotropic temperature factor, final conventional R factor and the list of the observed and calculated structure factors (F) are shown in Table 4. Conventional R factors of samples being 5-6 %, Pm3m is considered to be correct.

Table 4 Temperature factor, R factor and structure factors ($F_{obs.}$ and $F_{cal.}$)

X=0			X=0.1		
h k l	$F_{obs.}$	$F_{cal.}$	h k l	$F_{obs.}$	$F_{cal.}$
1 0 0	2.28	3.87	1 0 0	5.53	3.99
1 1 0	41.37	42.98	1 1 0	38.77	42.71
1 1 1	20.60	20.23	1 1 1	20.83	20.88
2 0 0	48.68	46.77	2 0 0	47.27	47.20
2 1 1	30.82	30.11	2 1 1	29.56	29.90
2 2 0	29.14	30.46	2 2 0	31.34	30.88
3 1 0	21.49	22.24	3 1 0	22.81	22.12
3 1 1	10.05	10.33	3 1 1	11.01	10.75
2 2 2	19.44	21.61	2 2 2	21.54	21.93
3 2 1	19.39	16.97	3 2 1	22.54	16.90
Sr: 2.00			Sr: 2.00		
Co: 4.00			Co: 4.00		
↳O: 7.58			Mn: 4.00		
R=5.4%			O: 6.78		
			R=5.3%		

X=0.5			X=0.8		
h k l	$F_{obs.}$	$F_{cal.}$	h k l	$F_{obs.}$	$F_{cal.}$
1 0 0	7.60	4.93	1 0 0	1.76	6.02
1 1 0	40.40	42.18	1 1 0	40.58	42.23
1 1 1	20.66	20.70	1 1 1	19.06	18.93
2 0 0	45.87	45.65	2 0 0	38.85	42.83
2 1 1	30.74	29.61	2 1 1	28.48	29.76
2 2 0	30.89	29.65	2 2 0	29.35	27.66
3 1 0	20.38	21.92	3 1 0	24.62	21.95
3 1 1	11.36	10.46	3 1 1	11.94	9.60
2 2 2	18.46	21.06	2 2 2	19.84	19.82
3 2 1	18.81	16.76	3 2 1	21.53	16.71

Sr: 2.00
Co: 4.00
Mn: 4.00
O: 8.25
R=5.8%

Sr: 2.00
Co: 4.00
Mn: 4.00
O:13.00
R=9.4%

X=1.0

h k l	$F_{obs.}$	$F_{cal.}$
1 0 0	5.89	5.83
1 1 0	38.54	40.93
1 1 1	24.14	22.13
2 0 0	46.22	45.32
2 1 1	28.93	28.54
2 2 0	28.01	29.46
3 1 0	21.12	21.11
3 1 1	10.41	11.23
2 2 2	19.44	20.89
3 2 1	19.57	16.15

Sr: 2.00

Mn: 4.00

O: 6.99

R=5.3%

Chapter 4 DISCUSSION

4-1) $SrCoO_{3-\delta}$ system

In the cubic perovskite structure, the ionic radius of Co^{4+} ion was calculated using the following simple equation,

$$r_{Co^{4+}} = 1/2(a_o - 2r_{O^{2-}}) \quad \text{--- (5)}$$

where $r_{O^{2-}} = 0.140$ nm. By putting the values of $a_o = 0.3836$ nm for $SrCoO_3$ into the equation (5), $r_{Co^{4+}}$ at the octahedral site was determined to be 0.0518 nm. Assigning the average ionic radius of the trivalent cobalt ion at the octahedral site to be 0.061 nm for the high spin state and 0.0525 nm for the low spin state as reported by Shannon and Prewitt (42), the tendency to decrease of the cell constant for $SrCoO_{3-\delta}$ was well understood to be caused by the decrease of the oxygen deficiency. Taguchi et al. (43) determined the ionic radius of the tetravalent cobalt ion using the result of the single crystal X-ray analysis for 2H-$BaCoO_3$ (44) with hexagonal symmetry. The crystal structure of $BaCoO_3$ was described in term of the hexagonal closed-packing BaO_3 layer and Co ions located in the oxygen octahedra as shown in Fig. 27. Within the BaO_3 layer, the O-O distance between the layers is 0.2787 nm, the O-O distance of 0.2513 nm within the layer is much shorter and these three oxygens forming a short O-O distance make a triangular plane sharing the face of the CoO_6 octahedra

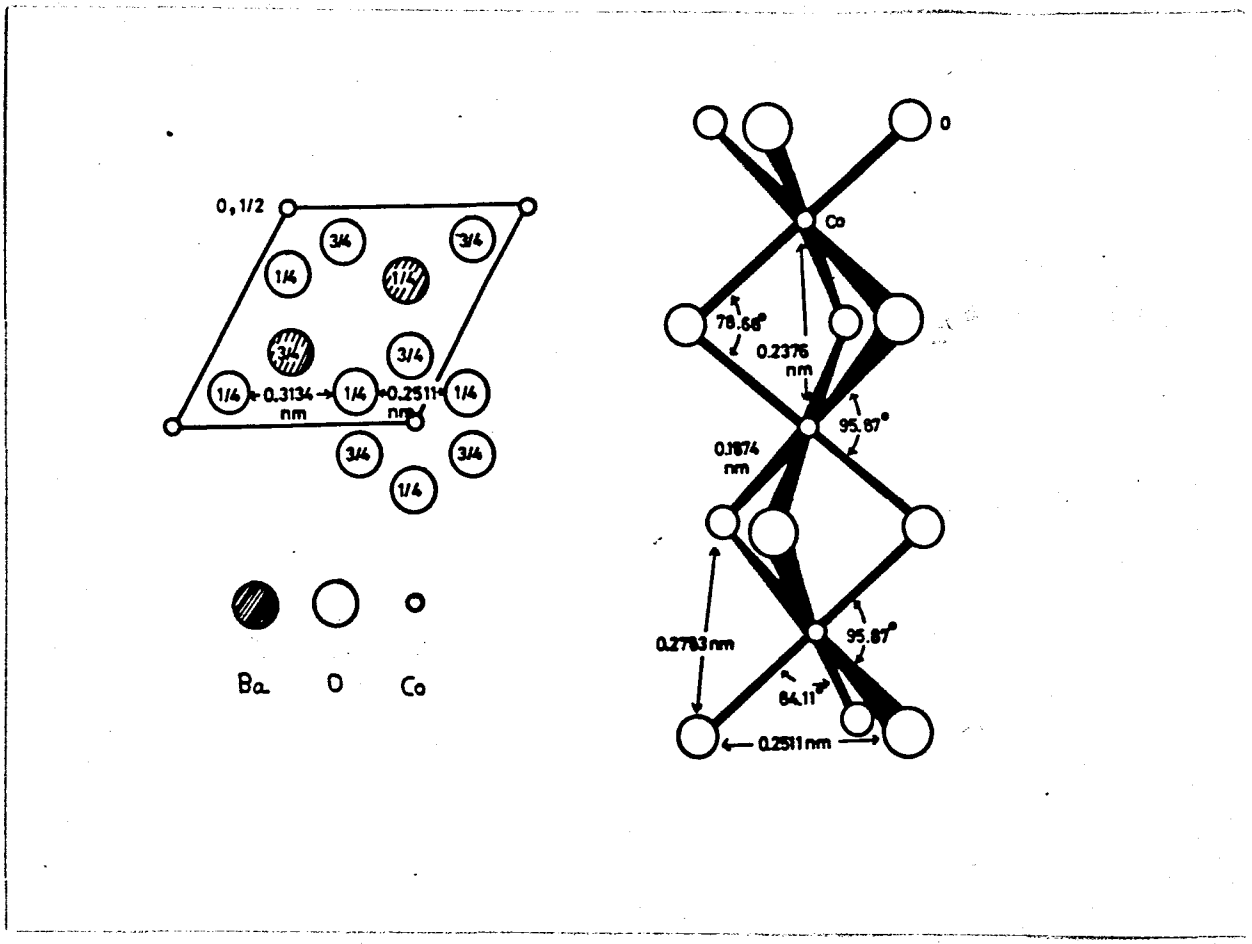

(a) (b)

Fig. 27 Crystal structure of $BaCoO_3$. (a) viewed along c. (b) anion chain.

columns. Co^{4+} ions in the columns face each other at a very short distance of 0.238 nm. This will produce a large electrostatic repulsion between the metal ions. As the oxygen atoms of face-sharing triangles mutually approach, the O ions screen the Coulomb interaction between Co^{4+} ions and weaken the repulsion.

Goldschmidt tolerance factor (t) is 1.046 in $SrCoO_3$ and 1.13 in $BaCoO_3$. For all compounds with the ideal cubic perovskite-type structure, the value of t lies between approximately 0.9 and 1.0, but for higher or lower values of t the hexagonal perovskite-type structure is found. This fact suggests that the cubic phase, rather than the hexagonal phase, is stable for $SrCoO_3$.

The observed magnetic momenta ($\bar{n}$) in the system $SrCoO_{3-\delta}$ is larger than calculated one. Raccah and Goodenough (24) pointed out that $\bar{n}$ in metallic $(La_{0.5}Sr_{0.5})CoO_3$ could be rationalized with an intermediate-spin model having localized t_2^5 configurations on each cobalt ion and an itinerant σ^* orbitals containing 0.5 electron per cobalt ion magnetized ferromagnetically. The model is schematically shown in Fig. 28. The average magnetic momenta of Co ion are given as follows,

$$\bar{n}=(X+2n)\mu_B \qquad \text{--- (6)}$$

where n is the number of σ^* orbital electrons per molecule, X is the composition in the system $(La_{1-X}Sr_X)CoO_3$. For X=0.5, the intermediate-spin configuration would be

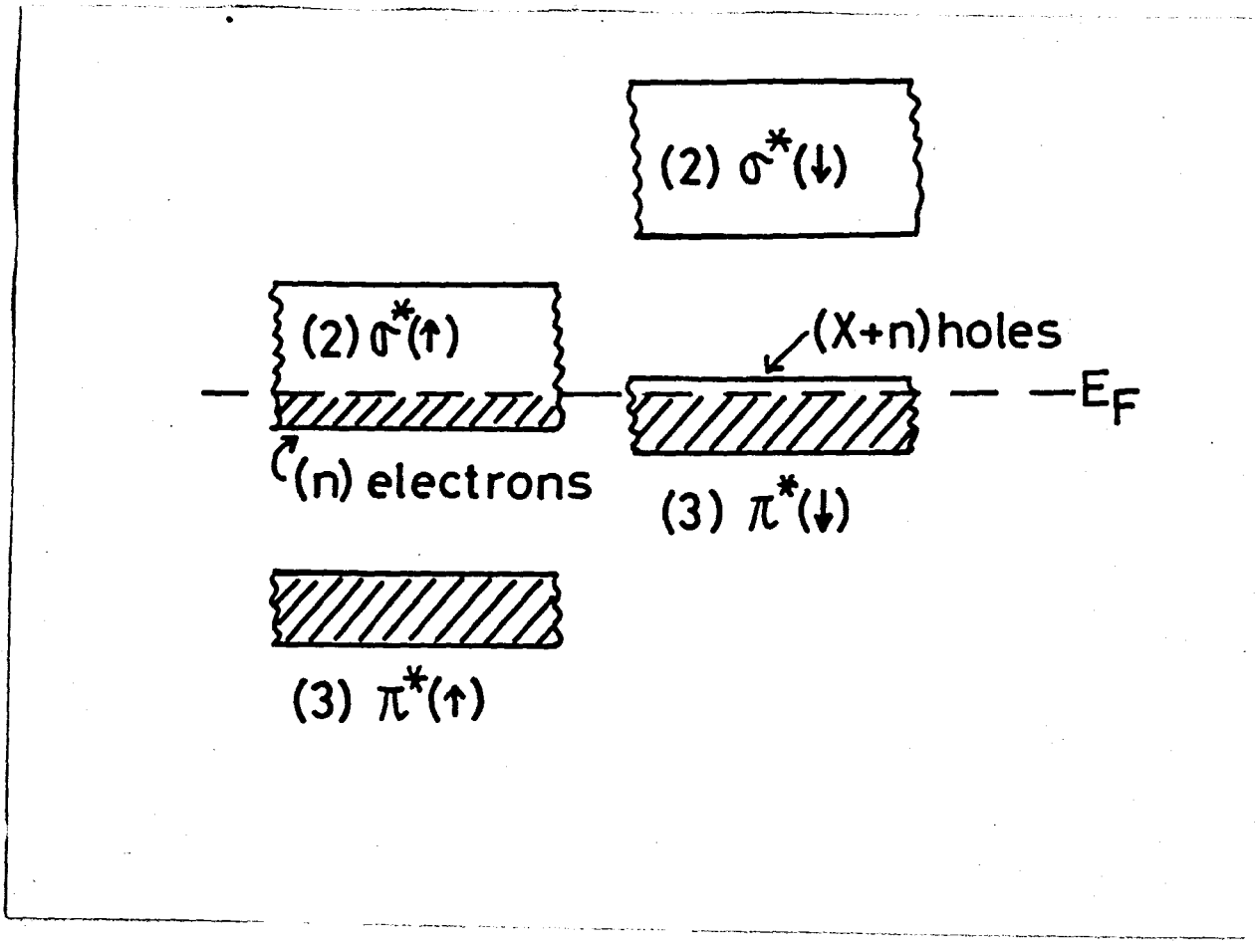

Fig. 28 Band model for $(La_{1-X}Sr_X)CoO_3$.

$\pi^{*5.0}\sigma^{*0.5}$. This model could account for the observed $\bar{n}$ in metallic $SrCoO_3$ if the itinerant σ^* orbital overlaps the localized t_2^5 level (or strongly correlated π^{*5} orbital). For g=2.0 and $\bar{n}$=1.6, the intermediate-spin configuration would be $\pi^{*4.7}\sigma^{*0.3}$. The magnetic moment ($\bar{n}$) of Co ion are given as follows,

$$\bar{n}=(1-2\delta+2n) \qquad \text{--- (7)}$$

where n is the number of up-spin σ^* orbital electrons per molecule. This model is schematically shown in Fig. 29. Fig. 30 shows the number of electrons in the σ^* and π^* orbitals calculated from the equation (7). The number of electrons in the π^* orbitals increases and those in the σ^* orbitals decreases with increasing the oxygen deficiency. This fact suggests that the increase of the oxygen deficiency would add electrons to the π^* orbitals more rapidly than those to the broad σ^* orbitals and the π^* orbitals shift downward relatively to the braod σ^* orbitals with increasing the oxygen deficiency. Increasing the oxygen deficiency in $SrCoO_{3-\delta}$, the number of electrons in the σ^* ($\uparrow$) orbitals and the π^* orbitals below E_F (Fermi energy) increases according to the function of $6-(1-2\delta)=5+2\delta$ calculated from the equation $3+n+(3-1+2\delta-n)$, and this would be confirmed by the results of the decrease of $\log\rho$ at 80K and 300K.

The itinerant-electron model mentioned above would also account for the change in Tc and T_θ with δ.

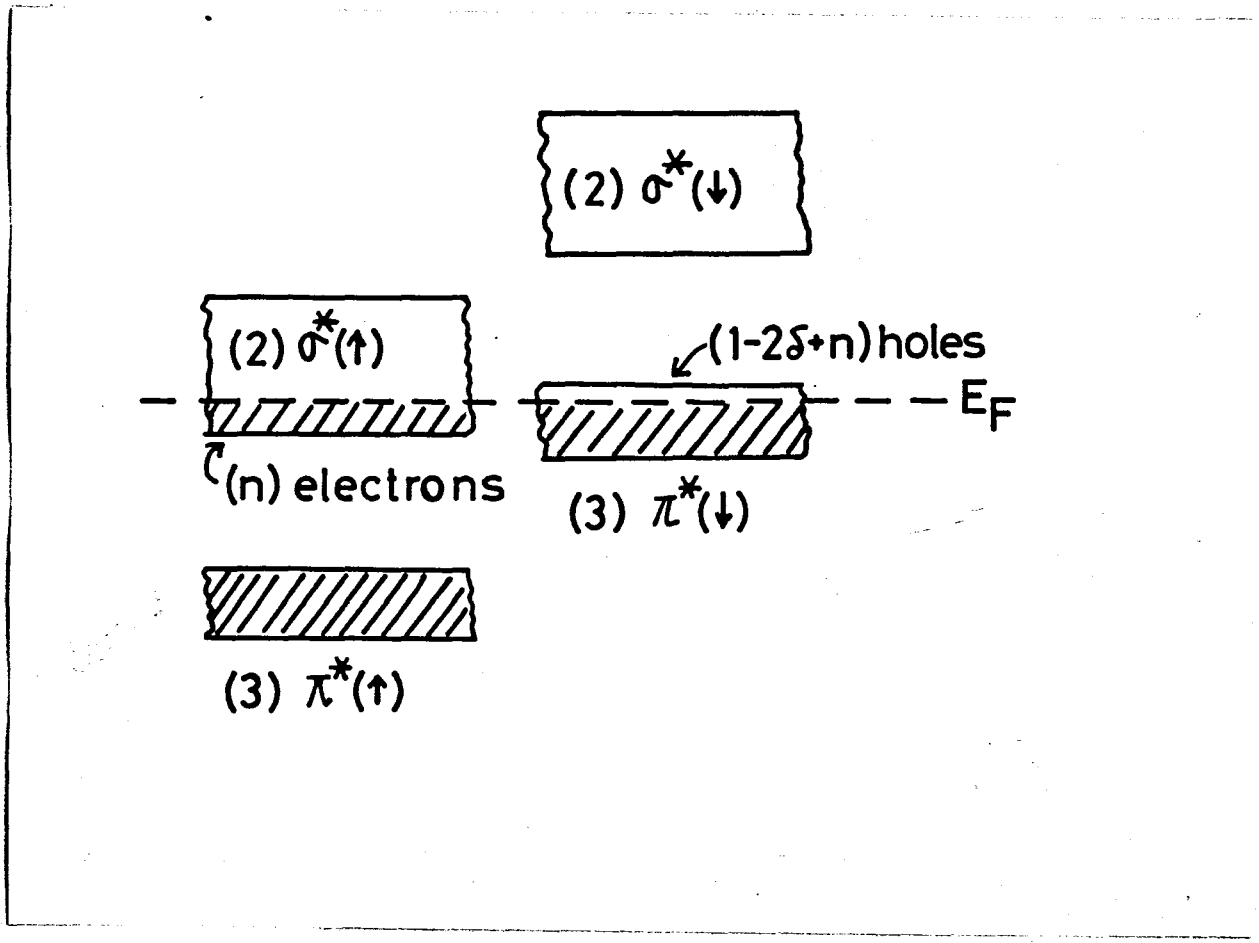

Fig. 29 Band model for $SrCoO_{3-\delta}$.

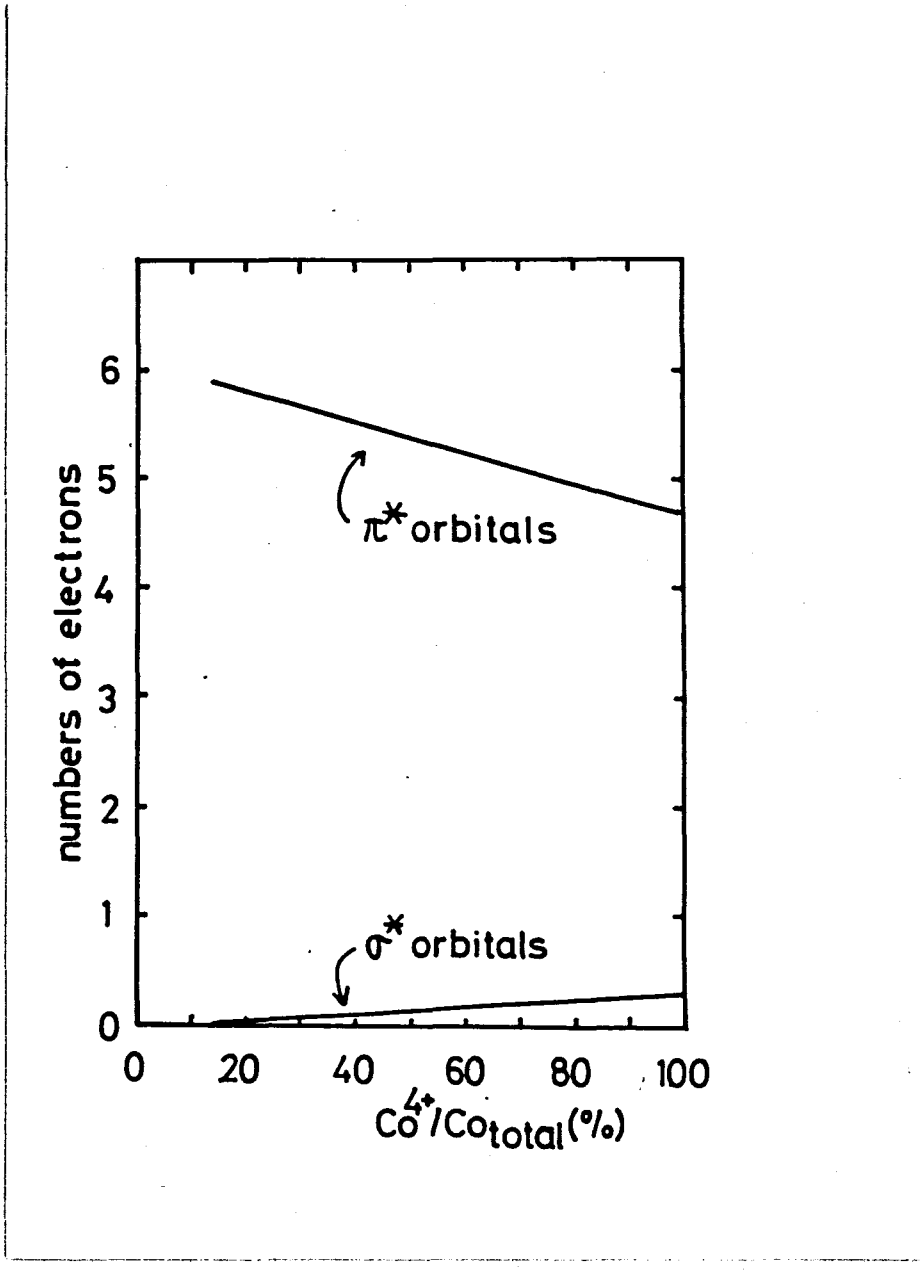

Fig. 30 Number of electrons vs. Co^{4+} content in the system $SrCoO_{3-\delta}$.

In case of ferromagnetic compounds, Tc and T_θ are expressed as follows,

$$Tc \approx T_\theta = 2Z|J|S(S+1)/2k \qquad \text{--- (8)}$$

where Z is the number of the nearest neighbor cations, $|J|$ is the effective exchange integral, S is the number of spin and k is the Boltzman constant. With increasing δ in $SrCoO_{3-\delta}$, the values of effective magnetic spin (S) of cobalt ions decrease, and Tc and T_θ decrease as shown in Figs. 5 and 7.

In the Mössbauer spectra measurement of the ferromagnet and the antiferromagnet, the angle between the direction of the spin and the gamma ray (θ) is important to examine the magnetic hyperfine interaction. In Table 5, the angular dependence of the various allowed transitions is shown. In case when external magnetic field is not applied, the direction of each spin is at random; $\overline{\cos^2\theta}=1/3$ and $\overline{\sin^2\theta}=2/3$. The ratio of the intensity is 3:2:1:1:2:3 as shown in Fig. 31. When the external magnetic field is applied parallel to the gamma ray direction and $\theta=0^\circ$, the transition $\Delta m=0$ vanishes; $\overline{\cos^2\theta}=0$ and $\overline{\sin^2\theta}=1$. The ratio of the intensity is 3:0:1:1:0:3. When the external magnetic field is applied parallel to the gamma ray direction and $\theta=90^\circ$, the angular terms in R shown in Fig. 31 was determined to be $\overline{\cos^2\theta}=1$ and $\overline{\sin^2\theta}=0$. The ratio of the intensity is 3:4:1:1:4:3.

The Mössbauer spectra of $Sr(Co_{0.99}{}^{57}Fe_{0.01})O_3$ in

Table 5 Angular dependence of various allowed transition.

transition	Δm	total	angular dependence
$3/2 \rightarrow 1/2$	-1	3	$9(1+\cos^2\theta)/4$
$-3/2 \rightarrow -1/2$	+1		
$1/2 \rightarrow 1/2$	0	2	$3\sin^2\theta$
$-1/2 \rightarrow -1/2$	0		
$-1/2 \rightarrow 1/2$	+1	1	$3(1+\cos^2\theta)/4$
$1/2 \rightarrow -1/2$	-1		

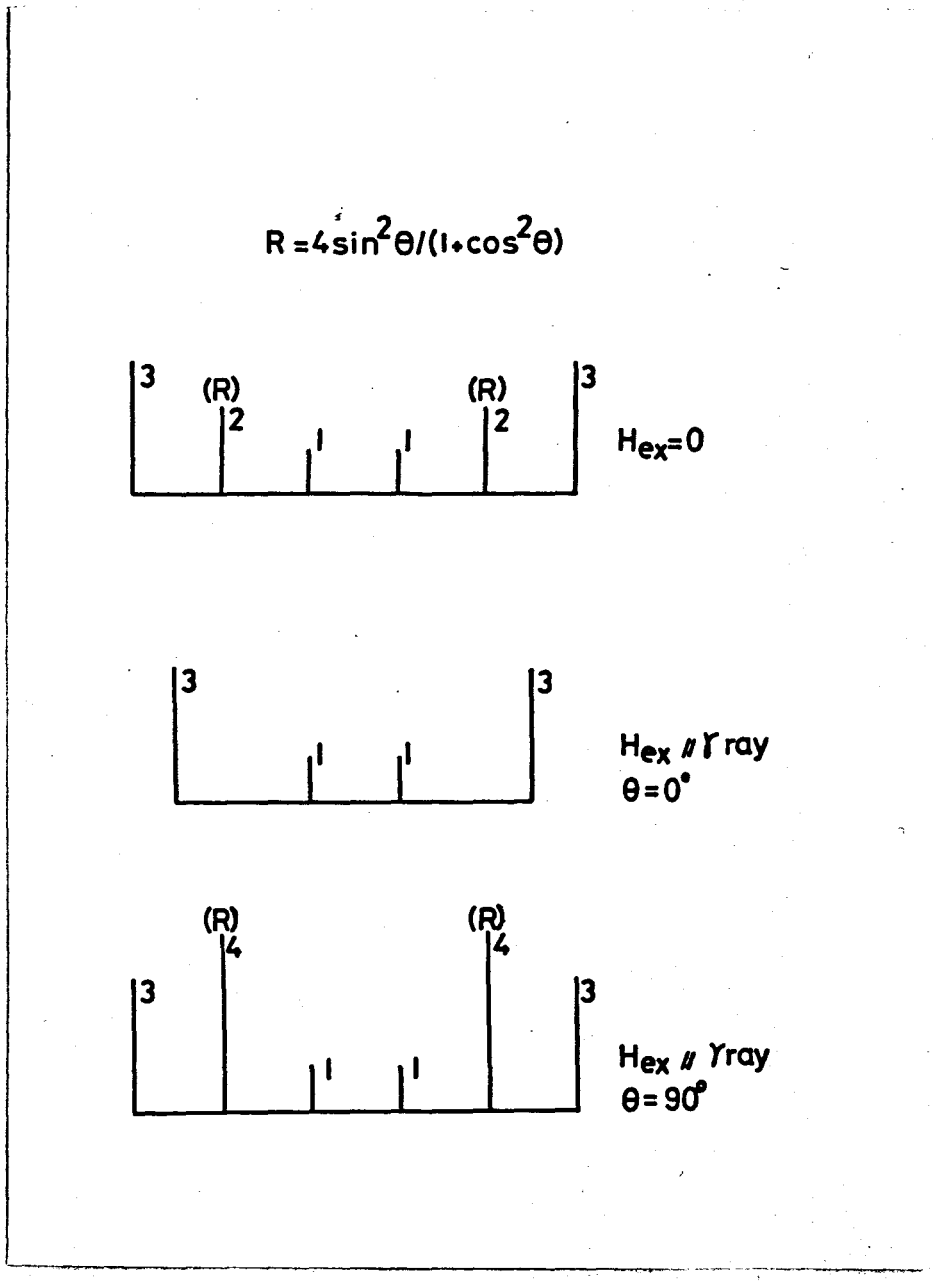

Fig. 31 Ratio of intensity for Mössbauer spectra.

case when the external magnetic field was applied parallel to the gamma ray direction are shown in Fig. 11. From the results of the intensity ratio of 3:0:1:1:0:3, it is clear that the direction of the spin of Fe^{4+} ion is parallel to the external magnetic field. The internal magnetic field of 296 kOe at 4.2K decreased by appling the magnetic field. From these results, it is expected that the spin structure of pure $SrCoO_3$ is suggested to be collinear.

Takeda and Watanabe investigated the magnetic properties of solid solution of $Sr(Co,Fe)O_3$ (20) and obtained the results shown in Fig. 32. From these data revealed the followings.

(1) The dilute Fe in $SrCoO_3$ couples ferromagnetically with the ferromagnetic matrix.

(2) Magnetization of the system has a maximum around the middle, X=0.5.

As shown in Fig. 11 at 4.2K, a magnetic hyperfine field of 296 kOe was observed. All Fe ions are confirmed to be in a single Fe^{4+} state. When an external magnetic field (45 kOe) was applied in parallel to the gamma ray direction, No.2 and No.5 lines disappeared nearly completely and the effective field was decreased. It is thus clear that the sign of the Fe^{4+} hyperfine field is negative. This fact is the first observation of Fe^{4+} ion in a ferromagnetic substance. The spin structure

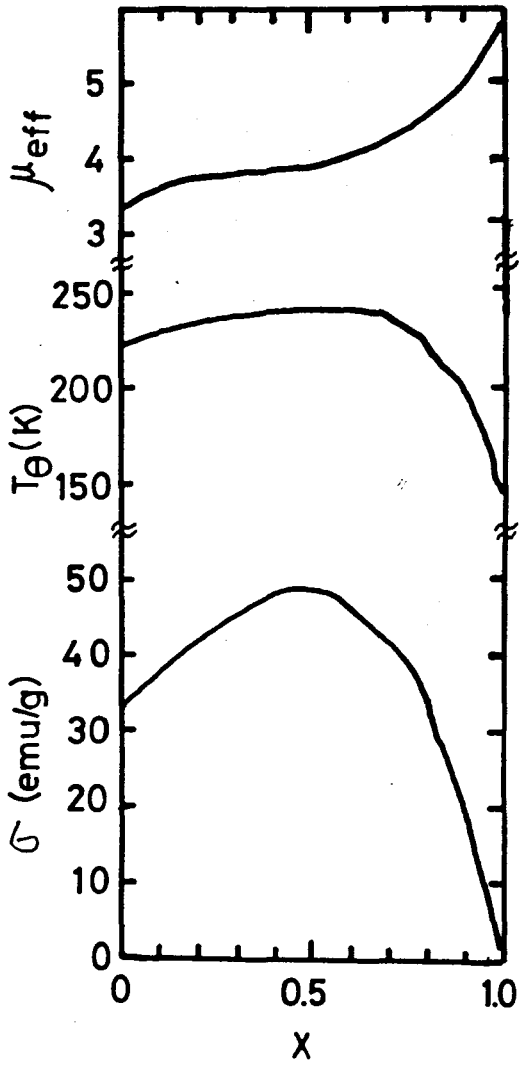

Fig. 32 Compositional dependence of μ_{eff}, T_θ and σ at a field of 6 kOe at 77K in the system $Sr(Co_{1-X}Fe_X)O_3$.

of pure $SrCoO_3$ is suggested to be collinear by the fact that the magnetic spin of impurity Fe has been oriented to the direction of external field.

The change of the magnetization shown in Fig. 32 is interpreted as follows. When the content of Fe in $SrCoO_3$ is small, the spin of iron couples ferromagnetic matrix. With increase of Fe content, antiferromagnetic coupling between Fe atoms becomes significant. Then the spin structure must be complicated. Partially or entirely, canted spin configuration might be realized and the magnetization curves eventually shows a maximum around X=0.5.

The change of the hyperfine field is rather small and the electronic structure of Fe^{4+} ion itself is almost the same in the whole composition range.

4-2) $(La_{1-X}Sr_X)CoO_3$ system

The distance between Co and O ions is 0.1918 nm for $SrCoO_3$ (X=1.0) and 0.1914 nm for $(La_{0.3}Sr_{0.7})CoO_3$ (X=0.7) as shown in Fig. 13. The ionic radius of Sr^{2+} ion is 0.144 nm and that of La^{3+} ion is 0.132 nm (42). Since the valence state of Co ion changes from tetravalent to trivalent due to the cation replacement of Sr^{2+} ion by La^{3+} ion, the average ionic radius of Co ions increases with decreaing X from 1.0 to 0.5. The tendencies of a small decrease of cell constant in the range of $0.7 \leqq X \leqq 1.0$ and of the increase of cell constant in the range of $0.5 \leqq X \leqq 0.7$ are understood as a result of the change of the average ionic radius for A cations (Sr^{2+} and La^{3+}) and B cations (Co^{3+} and Co^{4+}). In the former composition range of $0.7 \leqq X \leqq 1.0$, the decrease of the average distance between A cations results in the decrease of the cell constant and, in the range of $0.5 \leqq X \leqq 0.7$, the BO_6 packing strongly influences upon the cell constant.

Jonker (5) reported the compositional dependence of Tc and T_θ using the values of the magnetic superexchange interaction of Mn-O-Mn in the systems of $(La_{1-X}Sr_X)MnO_3$ and $(La_{1-X}Ca_X)MnO_3$. The change of the paramagnetic Curie temperature (T_θ) of solid solution of $(La_{1-X}Sr_X)CoO_3$ with the cubic phase forms a parabolic curve for the change of X as shown in Fig. 17. The interaction energy in term of the paramagnetic Curie temperature is expressed

as follows: θ_a for Co^{3+}-O-Co^{3+}, θ_b for Co^{3+}-O-Co^{4+} and θ_c for Co^{4+}-O-Co^{4+}. The fractions for Co^{3+} and Co^{4+} ions are then $(1-X)^2$ for Co^{3+}-O-Co^{3+}, $2X(1-X)$ for Co^{3+}-O-Co^{4+} and X^2 for Co^{4+}-O-Co^{4+}. If θ_a, θ_b and θ_c are considered as constants in a mixed crystal system, the compositional dependence of T_θ is calculated using the following equation.

$$T_\theta=(1-X)^2\theta_a+2X(1-X)\theta_b+X^2\theta_c \quad \cdots (9)$$

θ_a for $LaCoO_3$ is about -200K (45), θ_c for $SrCoO_3$ is 280K and T_θ is the observed value for each X. Using the above equation, the compositional dependence of T_θ is calculated by changing the values of θ_b. The best fitting results are shown in Fig. 33 and the following interactions were calculated.

$$Co^{3+}\text{-O-}Co^{3+} \sim -200K\ (\theta_a)$$
$$Co^{3+}\text{-O-}Co^{4+} \sim 440K\ (\theta_b)$$
$$Co^{4+}\text{-O-}Co^{4+} \sim 280K\ (\theta_c)$$

Since the magnetic superexchange interaction for Co^{3+}-O-Co^{4+} is the strongest one, Tc and T_θ increase with increasing X from 1.0 to 0.8 due to the substitution of Sr^{2+} ion by La^{3+} ion. However, as the content of La^{3+} ion increases, the superexchange interaction for Co^{3+}-O-Co^{4+} plays an important role for the total magnetic interaction, T_θ and Tc decrease monotonously.

From the results of the effective magnetic moment (μ_{eff}), it is considered that Co^{3+} ion is in the high spin state with the $(d\varepsilon)^4(d\gamma)^2$ and Co^{4+} ion is in the

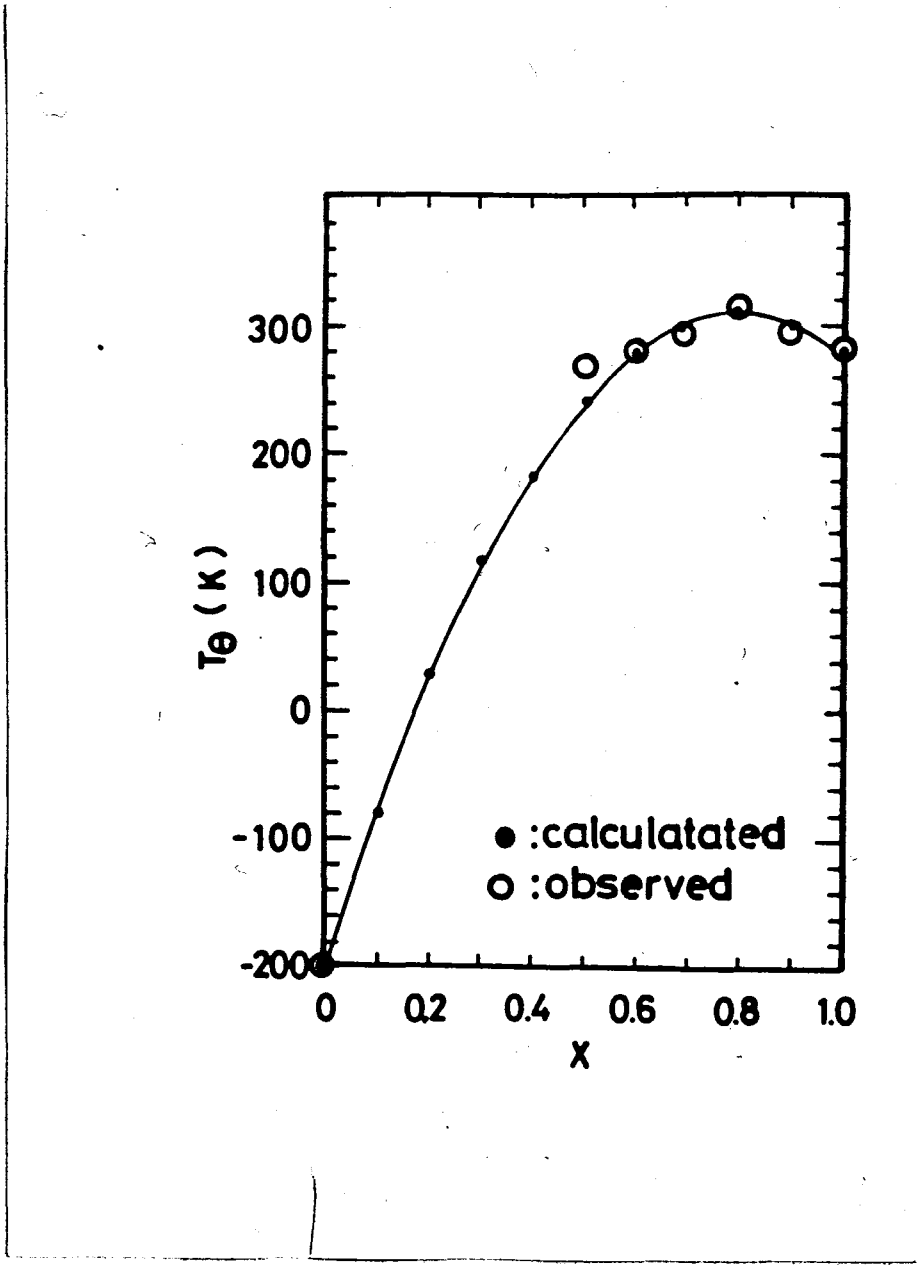

Fig. 33 Observed and calculated paramagnetic Curie temperature vs. composition in the system $(La_{1-X}Sr_X)CoO_3$.

low spin state with the $(d\varepsilon)^5(d\gamma)^0$. The magnetic moment of Co^{3+} ion is $\bar{n}=4$ and that of Co^{4+} ion is $\bar{n}=1$ from the electron configuration. The interaction energy in term of the magnetic moment ($\bar{n}$) is expressed as follows. $\bar{n}_a$ for Co^{3+}-O-Co^{3+}, $\bar{n}_b$ for Co^{3+}-O-Co^{4+} and $\bar{n}_c$ for Co^{4+}-O-Co^{4+}. The fractions for Co^{3+} and Co^{4+} ions are 1-X and X respectively. The fractions of neighboring pair are then $(1-X)^2$ for Co^{3+}-O-Co^{3+}, $2X(1-X)$ for Co^{3+}-O-Co^{4+} and X^2 for Co^{4+}-O-Co^{4+}. If $\bar{n}_a$, $\bar{n}_b$ and $\bar{n}_c$ are considered as constants in a mixed crystel system, the compositional dependence of $\bar{n}$ calculated using the following equation.

$$\bar{n}=(1-X)^2\bar{n}_a+2X(1-X)\bar{n}_b+X^2\bar{n}_c \qquad \text{--- (10)}$$

Since $LaCoO_3$ (X=0) is an antiferromagnet, the magnetic momenta align antiparallel each other and $\bar{n}_a$ is zero. Since $\bar{n}_c$ is equal to 4.0, $\bar{n}_b$ is calculated to be $\frac{1}{2}(\bar{n}_a+\bar{n}_c)=5/2$. Then, $\bar{n}$ is expressed as follows.

$$\bar{n}=0\times(1-X)^2+2X(1-X)5/2+X^2 \qquad \text{--- (11)}$$

The spontenious magnetization at OK (σ_o) is expressed as follows.

$$\sigma_o=1/M(5585\times\bar{n}) \qquad \text{--- (12)}$$

M is the mole weight of each cobaltite and 5585 is the constant calculated from (Avogadro Number)$\times\mu_B=(6.02\times10^{23})\times(9.28\times10^{-21})$. σ_o of each cobaltite is calculated from the following equation.

$$\sigma_o=1/M(5585\times(-4X^2+5X)) \qquad \text{--- (13)}$$

$\bar{n}$, M and σ_0 of each cobaltite are listed in Table 6. Calculated and observed σ_0 are plotted in Fig. 34. The broken line indicates the calculated values. In the range of $0.2 \leqq X \leqq 0.6$, the best fitting between calculated and observed σ_0 is recongnized. In the range of $0.7 \leqq X \leqq 1.0$, the observed σ_0 is larger about 5-10 emu/g than calculated σ_0, but the tendency of change in observed σ_0 is quite similar with the calculated σ_0.

This fact supports that the electron configuration of Co^{3+} and Co^{4+} ions calculated from the paramagnetic region is agreed with that from the ferromagnetic region. The presence of the maximum value of σ_0 at about X=0.8 is explained by the magnetic superexchange model proposed by Jonker (5) as well as Tc and T_θ.

To account for the ferromagnetism and metallic conductivity of $(La_{1-X}Sr_X)CoO_3$ $(0.5 \leqq X \leqq 1.0)$, the itinerant-electron model (24) was adopted. Fig. 35 shows the relation between X and the number of electrons in the σ^* and π^* orbitals. In the range of $0.5 \leqq X \leqq 0.8$, the number of electrons in the π^* orbitals decreases with increasing X. This fact suggests that increase of X would add electrons to the broad σ^* orbitals more rapidly than that of the π^* orbitals, and that the π^* orbitals shift upward relatively to the σ^* orbitals with increasing X. In the range of $0.8 \leqq X \leqq 1.0$, the number of electrons in the π^* orbitals increases with increasing X. But

Table 6 $\bar{n}$, M and σ_o for $(La_{1-X}Sr_X)CoO_3$.

X	$\bar{n}$	M	σ_o
0.2	0.84	235.59	19.91
0.3	1.14	230.45	27.63
0.4	1.36	225.33	33.71
0.5	1.50	220.19	38.04
0.6	1.56	215.07	40.51
0.7	1.54	209.94	40.97
0.8	1.44	204.81	39.27
0.9	1.26	199.68	35.24
1.0	1.00	194.55	28.71

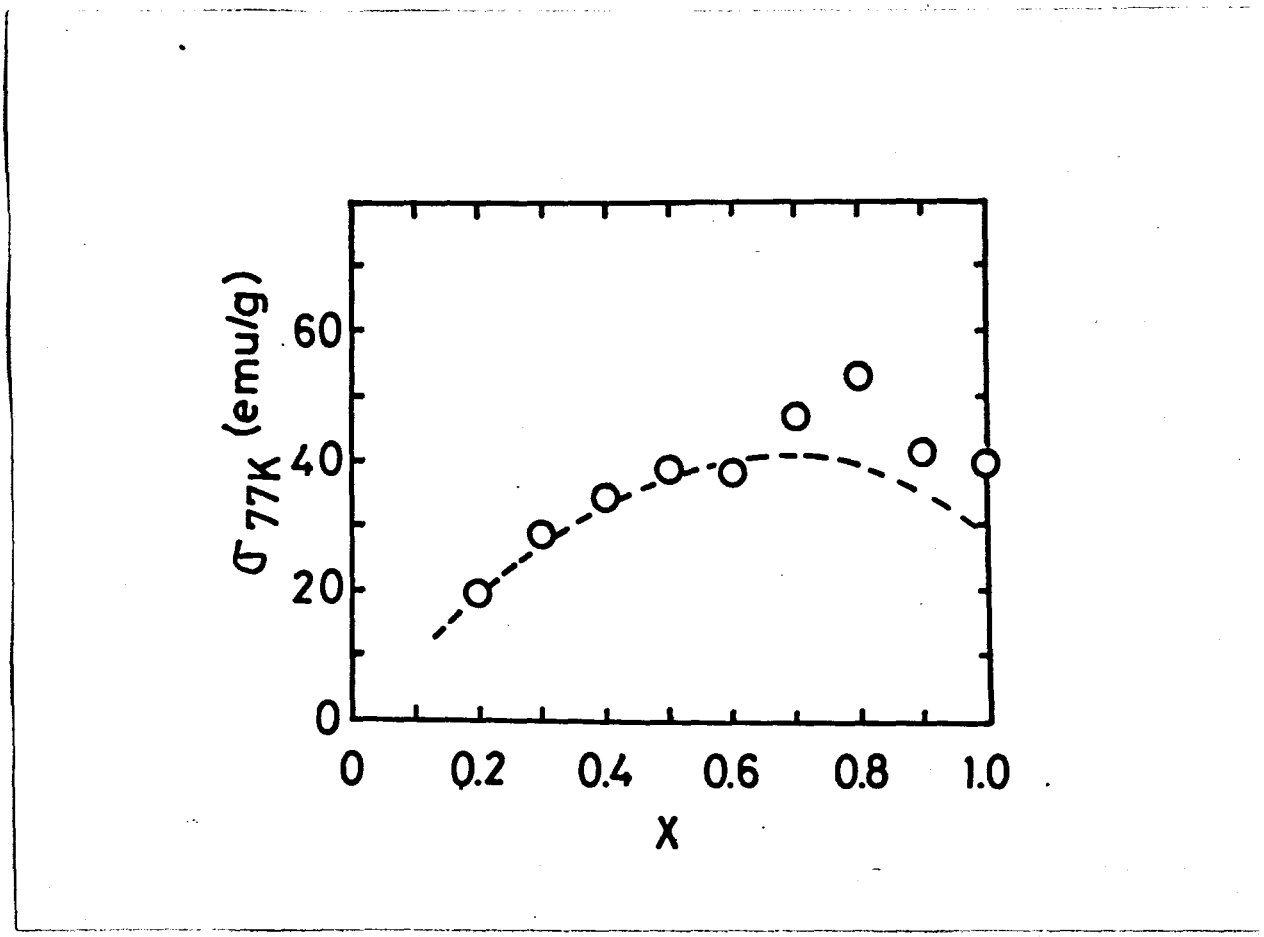

Fig. 34 Spontenious magnetization vs. composition in the system $(La_{1-X}Sr_X)CoO_3$.

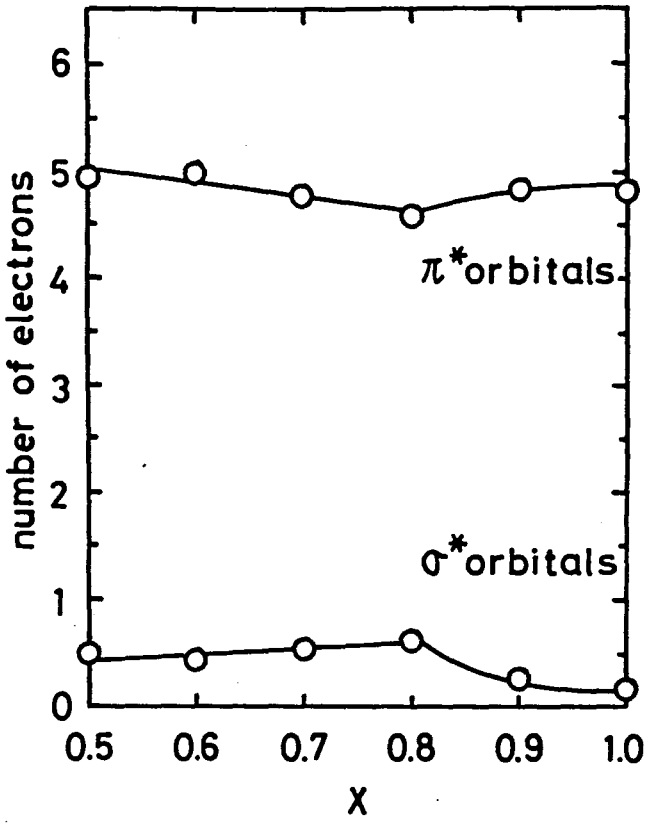

Fig. 35 Number of electrons vs. composition in the system $(La_{1-X}Sr_X)CoO_3$.

the number of electrons in the σ^* (↑) and π^* (↓) orbitals below E_F (Fermi energy) decreases according to the function of (6-X) calculated from the equation of 3+n+(3-X-n) (as shown in Fig. 28) in the range of $0.5 \leqq X \leqq 0.9$, and this idea would be confirmed on the basis of the results of $\log \rho$-X relation at 80K and 290K as shown in Fig. 20.

4-3) $Sr(Co_{1-X}Mn_X)O_3$ system

The change of cell constant with a break at X=0.3 for $Sr(Co_{1-X}Mn_X)O_3$ indicates that the ionic radius of Co^{4+} ion located at octahedral site changes due to the change of spin state from low to high with increasing X as shown in Fig. 26.

The isotropic temperature factor of oxygen for X=0.1 is nearly equal to that for X=0 and X=1.0, but that for X=0.5 or 0.8 is larger than that for X=0 and 1.0. The large isotropic temperature factors for X=0.5 and 0.8 would be corresponded to the change of spin state in Co^{4+} ion.

$MnFe_2O_4$ has the cubic and normal spinel structure. Using X-ray method, Červinka et al. examined whether the octahedra containing Mn^{2+} ion ($3d^5$) is tetragonally distorted or have cubic symmetry (46). From the large isotropic temperature of $MnFe_2O_4$, they concluded that the existence of tetragonally deformed octahedra was caused by cooperative Jahn-Teller distortion of Mn^{2+} ion. In the system of $Sr(Co_{1-X}Mn_X)O_3$, it is considered that the large isotropic temperature factor of oxygen is caused by the difference of Me^{4+}-O distance. The electronegativities (χ) of Mn^{4+} ion with the $(d\varepsilon)^3(d\gamma)^0$, Co^{4+} ion with the $(d\varepsilon)^5(d\gamma)^0$, and Co^{4+} ion with the $(d\varepsilon)^3(d\gamma)^2$ are 5.61, 2.92 and 3.00 respectively (47). Since the difference between Mn^{4+} and O^{2-} ion

($\Delta\chi \approx 2.1$) is larger than that between Co^{4+} and O^{2-} ion ($\Delta\chi \approx 0.5$), it is expected that Mn^{4+}-O bond is stronger than Co^{4+}-O bond. The electron cloud of oxygen for X=0.5 and 0.8 spreads more widely than that of X=0, 0.1 and 1.0. This is schematically illustrated in Fig. 36. This model corresponds to the large isotropic temperature factor for X=0.5 and 0.8.

In the range of $0 \leq X < 0.3$, the increase of a-axis is considered to be based on the Vegard rule; the distance of Co^{4+} (low spin state)-O is 0.1918 nm (33) and that of Mn^{4+}-O is 0.1940 nm, assuming that Mn^{4+} ion in $Sr(Co_{1-X}Mn_X)O_3$ normally behaves as a tetravalent ion as in the case of Mn^{4+} ion in Mg_6MnO_8, $ZnMn_3O_7 \cdot 3H_2O$ and $DyMn_2O_5$ (42). The variation of a-axis with the increase of Mn^{4+} ion content is represented as follows.

$$a = 2(r_{Mn-O}X + r_{Co-O}(1-X))$$
$$= 2(0.1940X + 0.1918(1-X)) \quad \text{--- (14)}$$

a-axis expands with increasing X. Consequently, the electron state of Co^{4+} ion in high spin state becomes to be more stable than that in low spin state, because the ionic radii of Co^{4+} ion in high spin state is larger than that in low spin state as well as for other transition metal ions.

The distance of Mn^{4+}-O in cubic perovskite $SrMnO_3$ is 0.1905 nm (15). In the perovskite type oxides, the bonding between manganese and oxygen is stronger than

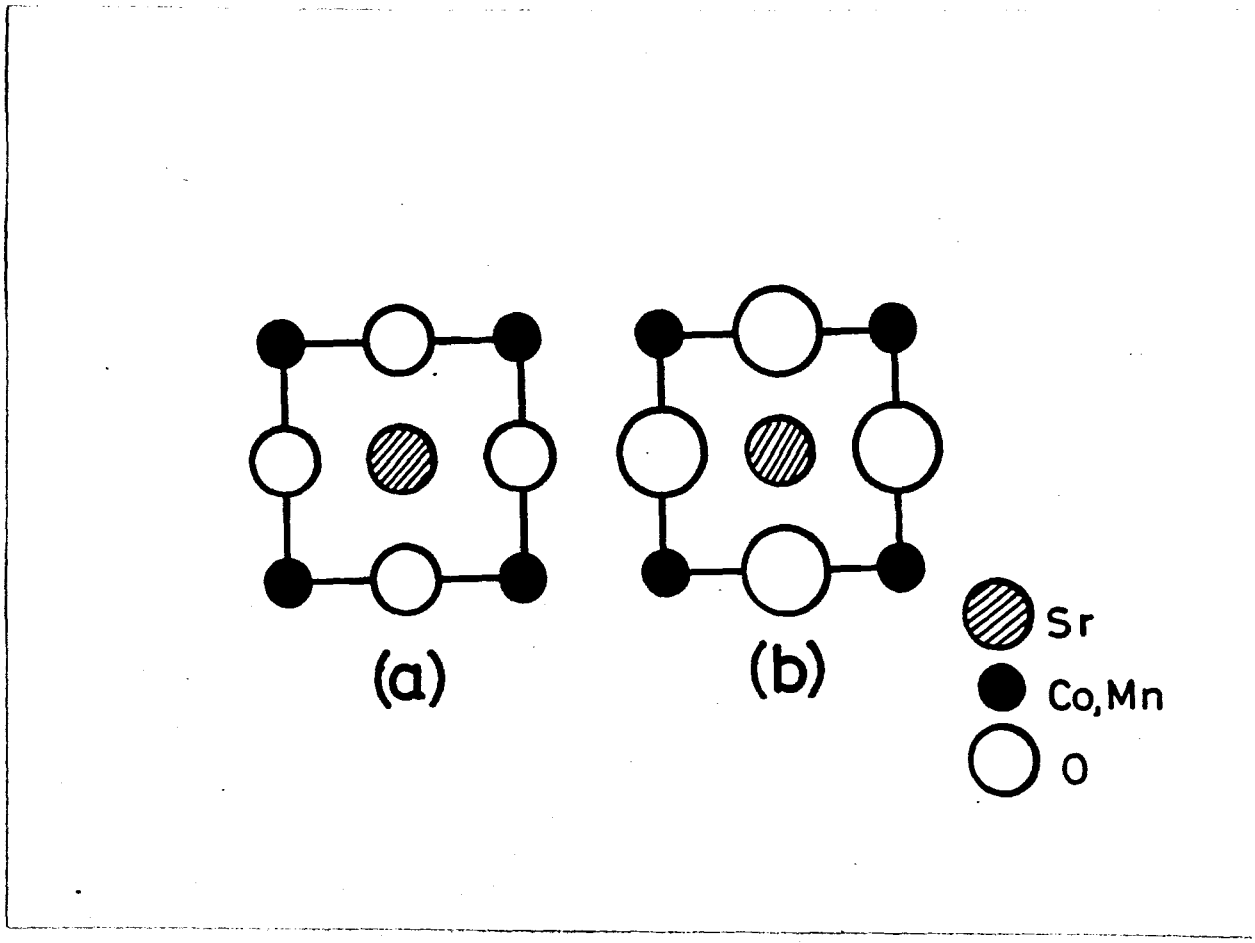

Fig. 36 The model of (110) plane. (a) X=0, 0.1 and 1.0. (b) X=0.5 and 0.8.

that in manganese oxides with a different crystal structure such as Mg_6MnO_8, $ZnMn_3O_7{\cdot}3H_2O$ and $DyMn_2O_5$.

In the range of $0.3 \leqq X \leqq 1.0$, the distance of Mn^{4+}-O decreased to 0.1905 nm. The variation of a-axis with the increase of Mn^{4+} ion content is represented as follows.

$$a=2(r_{Mn-O}X+r_{Co-O}(1-X))$$
$$=2(0.1905X+0.1935(1-X)) \quad \text{--- (15)}$$

Where, 0.1935 nm is the distance between Co^{4+}(high spin state)-O calculated from Fig. 21.

It is concluded that the volumes of CoO_6 and MnO_6 octahedra connected to each other with oxygens of the apex of the octahedron are equal in the range of $0 \leqq X < 0.3$ due to the small isotropic temperature factor of oxygen. In the range of $0.3 \leqq X \leqq 1.0$, the volumes of CoO_6 and MnO_6 octahedra are not equal but distributes statistically due to the large isotropic temperature factor of oxygen. The stability of Co^{4+} ion with high spin state in $Sr(Co_{1-X}Mn_X)O_3$ would be caused by the large CoO_6 octahedra.

The value of the effective magnetic moment at 0K for $SrMnO_3$ (14) is indicated as $\bar{n}=2.6\pm0.2\mu_B$. The deviation of $\bar{n}$ from $3.0\mu_B$, which is the theoretical value for Mn^{4+} ion ($3d^3$), is attributed to the electron transfer from Mn^{4+} ion to oxygen ion. From the results of the effective magnetic moment (μ_{eff}) shown in Fig. 26 and the spontenious magnetic moment σ_0 estimated using

the σ-T curve shown in Fig. 23, it is considered that the spin state of Co^{4+} ion changes from low to high at about X=0.3. The change of spin state in Co^{4+} ion is strongly influenced by cell constant and magnetic properties.

The magnetic superexchange interactions of Co^{4+}-O-Co^{4+}, Co^{4+}-O-Mn^{4+} and Mn^{4+}-O-Mn^{4+} in the system of $Sr(Co_{1-X}Mn_X)O_3$ were calculated by the same method described in the $(La_{1-X}Sr_X)CoO_3$ system. The interaction energy in term of T_θ are expressed as follows; θ_a for Co^{4+}-O-Co^{4+}, θ_b for Co^{4+}-O-Mn^{4+} and θ_c for Mn^{4+}-O-Mn^{4+}. The fractions for Co^{4+} and Mn^{4+} ions are 1-X and X respectively. The fractions of neighboring pair are $(1-X)^2$ for Co^{4+}-O-Co^{4+}, $2X(1-X)$ for Co^{4+}-O-Mn^{4+} and X^2 for Mn^{4+}-O-Mn^{4+}. If θ_a, θ_b and θ_c are considered to be constant in the solid solution samples, the compositional dependence of T_θ are calculated using the following equation.

$$T_\theta=(1-X)^2\theta_a+2X(1-X)\theta_b+X^2\theta_c \qquad \text{--- (16)}$$

Where, θ_a of $SrCoO_3$ is about 280K, θ_c of $SrMnO_3$ is about -750K (40) and T_θ is the observed value for each X. Using the above equation, the compositional dependence of T_θ is calculated by changing the values of θ_b. The best fitting results is shown in Fig. 37. In the range of $0 \leqq X < 0.3$, the following interactions were calculated.

Co^{4+}(low spin state)-O-Co^{4+}(low spin state),

$\sim$ 280K

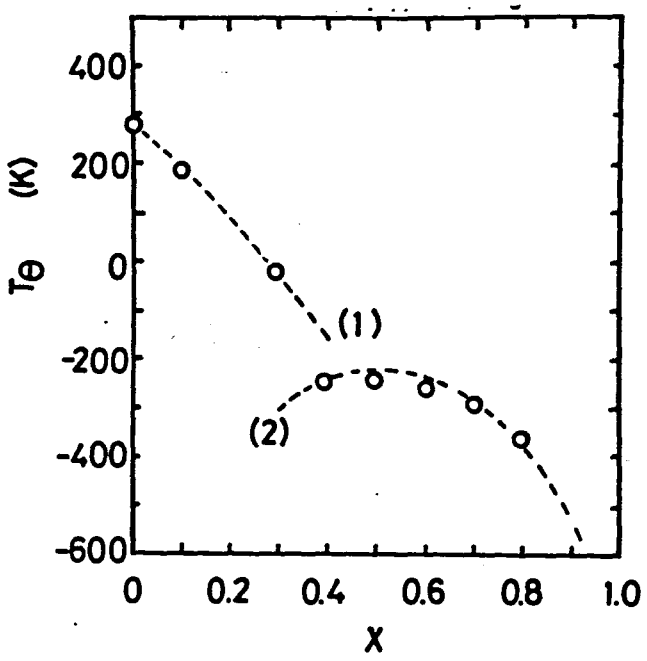

Fig. 37 Paramagnetic Curie temperature vs. composition in the system $Sr(Co_{1-X}Mn_X)O_3$.

Co^{4+}(low spin state)-O-Mn^{4+} $\sim$ -146K

Mn^{4+}-O-Mn^{4+} $\sim$ -750K

In the range of $0.3 \leqq X \leqq 1.0$,

Co^{4+}(high spin state)-O-Co^{4+}(high spin state) $\sim$ -1080K

Co^{4+}(high spin state)-O-Mn^{4+} $\sim$ 420K

Mn^{4+}-O-Mn^{4+} $\sim$ -750K

Since the magnetic superexchange interaction for Co^{4+}-O-Co^{4+} is ferromagnetic and that for Co^{4+}-O-Mn^{4+} or Mn^{4+}-O-Mn^{4+} is antiferromagnetic in the range of $0 \leqq X < 0.3$, T_θ, Tc and σ_o decrease with increasing X. In the range of $0.3 \leqq X \leqq 1.0$, although the magnetic superexchange interaction for Co^{4+}-O-Mn^{4+} is ferromagnetic, those for Co^{4+}-O-Co^{4+} and Mn^{4+}-O-Mn^{4+} are strongly antiferromagnetic.

4-4) Co^{4+} ion in octahedral environment

The spin states of Co^{4+} and Co^{3+} ions in $SrCoO_{3-\delta}$, $(La_{1-X}Sr_X)CoO_3$ and $Sr(Co_{1-X}Mn_X)O_3$ are discussed from their magnetic and electrical properties. In $SrCoO_{3-\delta}$ system, both Co^{3+} and Co^{4+} ions were in low spin state. In $(La_{1-X}Sr_X)CoO_3$ system, Co^{4+} ion was in low spin state and Co^{3+} ion was in high spin state. And in $Sr(Co_{1-X}Mn_X)O_3$ system, the spin state of Co^{4+} ion changed from low to high at X=0.3.

The crystal structure of the cubic perovskite oxides (ABO_3) is shown in Fig. 1. The distance between B cation and oxygen is a/2 nm (a: cell constant), and that between B and B cations is $\sqrt{2}a/2$ nm. From the crystallographic results, it is considered that the electron of B cation is not easily affected by other B cations. The difference of the spin state in Co^{3+} ion in the system of $SrCoO_{3-\delta}$ and $(La_{1-X}Sr_X)CoO_3$ suggests that A cation plays a significant role to determine the electron configuration of the other cations. Since the ionic radii of La^{3+} ion is 0.132 nm and that of Sr^{2+} ion is 0.144 nm (42), it is expected that the bonding between La^{3+} and O^{2-} ions is stronger than that between Sr^{2+} and O^{2-} ions. Increasing La^{3+} ion content in $(La_{1-X}Sr_X)CoO_3$, it is considered that the electron cloud of $2P_\pi$ in oxygen would be attracted to La^{3+} ion and Co^{3+} ion with high spin state would be stabilized in the octahedral site.

Though the ionic radii of Co^{3+} ion with high spin state is larger by ca. 0.01 nm than with low spin state, Co^{3+} ion with high spin state is stable at the octahedral site in case of brownmillerite type $Sr_2Co_2O_5$ (34).

The crystal structure of $Sr_2Co_2O_5$ is shown in Fig. 38 and the cell constants are a=0.5572 nm, b=1.573 nm and c=0.5468 nm. $Sr_2Co_2O_5$ is an antiferromagnet with the Néel temperature of 570K (34). From the neutron diffraction study, the magnetic structure is G-type and the magnetic moment of Co^{3+} is $3.3\pm0.5\mu_B$ at liquid nitrogen temperature.

In case of $SrCoO_{3-\delta}$ system, however, there are no other A cation whose electronegativity is larger than that of Sr^{2+} ion. Since Co^{3+} ion is only introduced by the existence of oxygen deficiency, it is considered that the spin state of Co^{3+} ion is directly influenced by the crystal field of mother matrix $SrCoO_3$.

The change of spin state in Co^{4+} ion occured in $Sr(Co_{1-X}Mn_X)O_3$ system. This change is caused by Mn^{4+} ion. The electronegativity of Mn^{4+} ion is stronger than that of Co^{4+} ion (Mn^{4+}:χ=5.61, Co^{4+}:χ=3.00). In the range of $0.3 \leqq X \leqq 1.0$, the oxygen located at the chain of Co^{4+}-O-Mn^{4+} deviated from the center, i.e. large CoO_6 octahedra and smaller MnO_6 octahedra, which were connected each other with oxygens of the apex of the octahedron, were distributed statistically.

Goodenough introduced the idea of the covalency

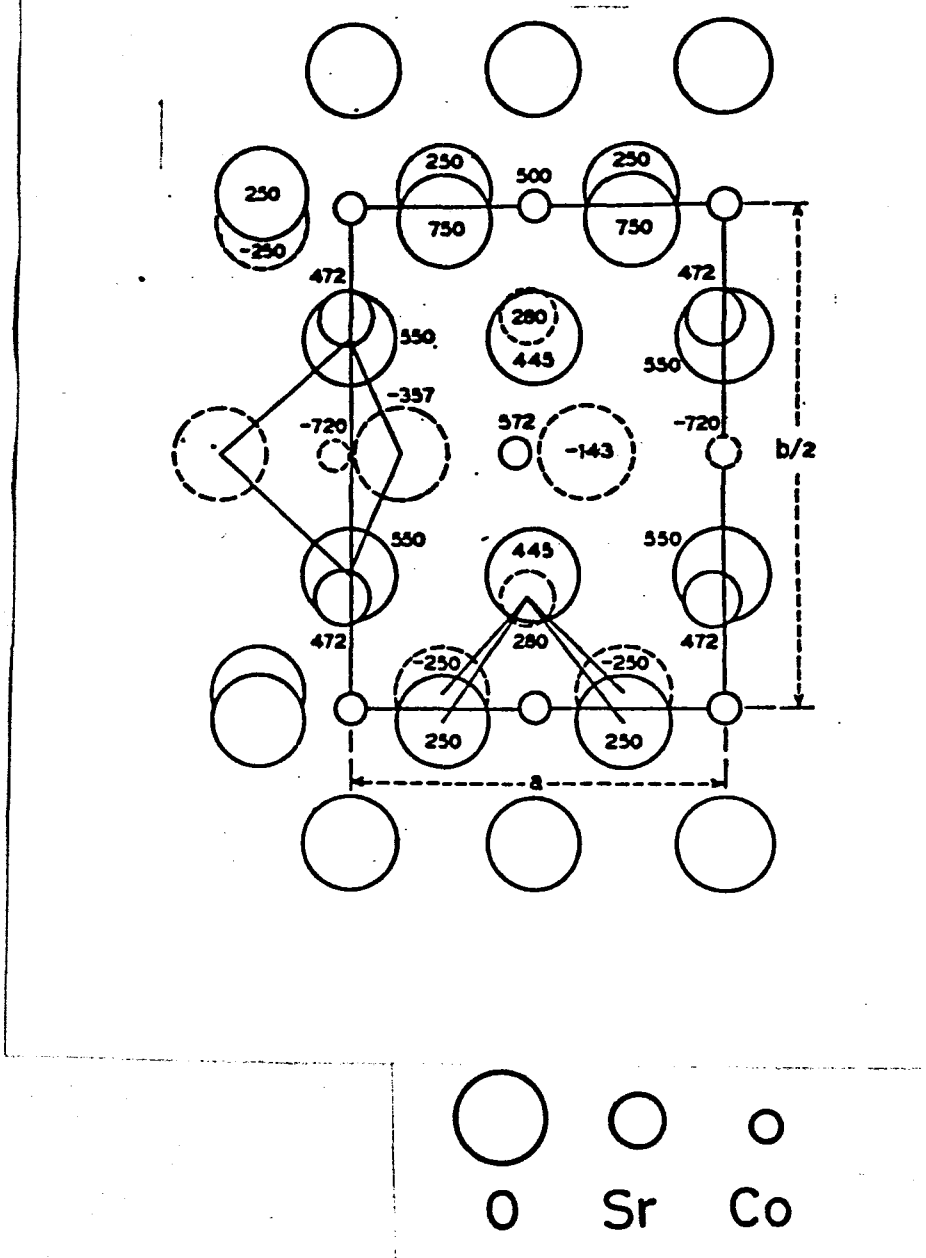

Fig. 38 Structure of brownmillerite.

criterion for localized vs. collective electrons in oxides with the perovskite structure(49,50,51). In many oxides, the outer d electrons are not localized magnetic electrons but collective metallic electrons either as a result of cation-sublattice band formation or of covalent mixing between anion P and cationic d state. The cation-sublattice band formation dose not take place in oxides with perovskite structure. A criterion for localized vs. collective electrons are defined as follow; where the overlap integral (Δ) is large enough, it is necessary to introduce a collective-electron theory, while, where it is small, the localized-electron theory is correct. The critical overlap integral is defined as Δ_c. If $\Delta<\Delta_c$, localized-electron theory is applied and , if $\Delta>\Delta_c$, collective-electron theory is applied.

For metallic perovskite oxides, collective-electron theory is applied as follows; oxides have a partially filled σ^* band because $\Delta^{\sigma}_{cac}>\Delta_c$. Where $\Delta^{\pi}_{cac}<\Delta_c<\Delta^{\sigma}_{cac}$, t^*_{2g} holes may simultaneously exist, and the localized orbital of α and β spins at a given cation are split by Δ_{ex}. In this case, the σ^*-band orbitals would also split by intra-atomic exchange, and then orbitals having α spin became more stable than those having β spin. This result is illustrated in Fig. 39.

The band model for metallic $SrCoO_{3-\delta}$ and $(La_{1-X}Sr_X)CoO_3$ is considered as shown in Fig. 40.

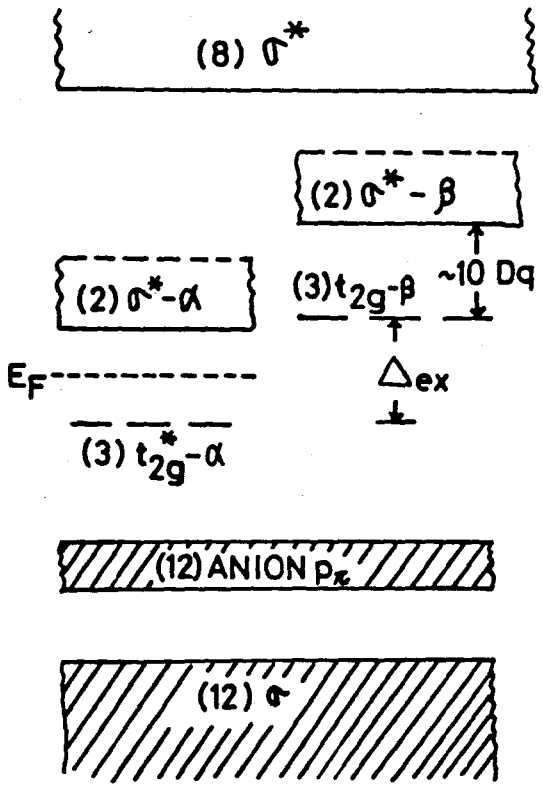

Fig. 39 Band model for $LaCrO_3$.

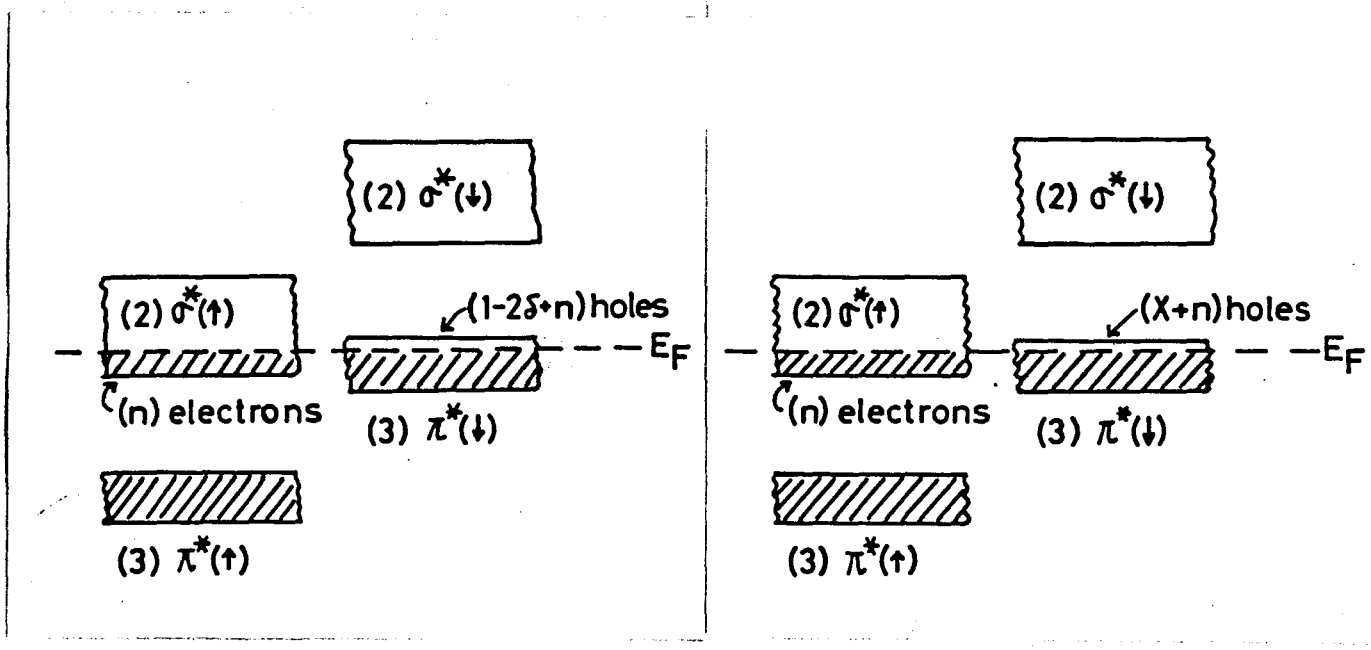

(a) $SrCoO_{3-\delta}$ (b) $(La_{1-X}Sr_X)CoO_3$

Fig. 40 Band model of $SrCoO_{3-\delta}$ and $(La_{1-X}Sr_X)CoO_3$.

In $SrCoO_{3-\delta}$ system, the number of electrons in the π^* orbitals increases and that in the σ^* orbitals decreases with increasing oxygen deficiency. This fact suggests that the increase of oxygen deficiency would add electrons to the π^* orbitals more rapidly than those to the broad σ^* orbitals and the π^* orbitals shift downward relatively to the broad σ^* orbitals with increasing oxygen deficiency. Increasing oxygen deficiency, the number of electrons in the σ^* ($\uparrow$) orbitals and π^* orbitals below E_F increases and this would be confirmed by the results of the decrease of $\log\rho$ at 80K and 300K.

In $(La_{1-X}Sr_X)CoO_3$ system, the number of electrons in the π^* orbitals decreases with increasing X in the range of $0.5 \leqq X \leqq 0.8$. This fact suggests that increase of X would add electrons to the broad σ^* orbitals more rapidly than that of the π^* orbitals, and that the π^* orbitals shift upward relatively to the σ^* orbitals with increasing X. In the range of $0.8 \leqq X \leqq 1.0$, the number of electrons in the π^* orbitals decreases with increasing X. Increasing X, the number of electrons in the σ^* ($\uparrow$) orbitals and π^* ($\downarrow$) orbitals below E_F decreases in the range of $0.5 \leqq X \leqq 0.9$, and this would be confirmed by the results of the increase of $\log\rho$ at 80K and 290K.

SUMMARY

Results and consideration in this paper are summarized as follows:

(1) Cubic perovskite type $SrCoO_{3-\delta}$ ($0<\delta<0.5$) were synthesized under various high oxygen pressures. Using the present $SrCoO_{3-\delta}$ with a fully controlled oxygen deficiency, it was found that the decrease of cell constant and increase of Tc, T_θ, σ and μ_{eff} are closely related with the Co^{4+} ion content.

(2) From the results of Mössbauer effect measurements of ^{57}Fe doped $SrCoO_3$, the spin structure of pure $SrCoO_3$ was suggested to be collinear by the fact that the magnetic spin of impurity Fe had been oriented to the direction of the external field. It is also clear that the sign of the Fe^{4+} hyperfine field is negative.

(3) Cubic perovskite type $(La_{1-X}Sr_X)CoO_3$ ($0.5 \leqq X \leqq 1.0$) were synthesized under high oxygen pressures. From the magnetic measurements, all samples were ferromagnetic. The spin state of Co^{3+} ion was in high spin state and that of Co^{4+} ion was in low spin state.

(4) Magnetic superexchange interaction for Co^{3+}-O-Co^{4+} was stronger than those for Co^{4+}-O-Co^{4+} and for Co^{3+}-O-Co^{3+} in $(La_{1-X}Sr_X)CoO_3$. And the presence of maximum values of Tc, T_θ and σ_{77K} at X=0.8 was explained by the contribution of these magnetic superexchange interaction.

(5) Both $SrCoO_{3-\delta}$ and $(La_{1-X}Sr_X)CoO3$ were good conductors and had metallic temperature coefficient. The magnetic transition were independent on the electrical conductivities. The logarithm specific resistivities ($\log\rho$) at 77K and 300K monotonously increased with increasing Co^{4+} ion content.

(6) Cubic perovskite type $Sr(Co_{1-X}Mn_X)O_3$ were synthesized under high oxygen pressures. a-axis had a maximum value at X=0.3. $Sr(Co_{1-X}Mn_X)O_3$ were ferromagnetic in the range of $0 \leqq X < 0.3$ and antiferromagnetic in the range of $0.3 \leqq X \leqq 1.0$. The spin state of Co^{4+} ion changed from low to high at X=0.3.

(7) The magnetic superexchange interaction for Co^{4+}-O-Co^{4+} was ferromagnetic and those for Co^{4+}-O-Mn^{4+} and Mn^{4+}-O-Mn^{4+} were antiferromagnetic in the range of $0 \leqq X < 0.3$. In the range of $0.3 \leqq X \leqq 1.0$, the superexchange interaction for Co^{4+}-O-Mn^{4+} was ferromagnetic and those for Co^{4+}-O-Co^{4+} and Mn^{4+}-O-Mn^{4+} were antiferromagnetic in the system $Sr(Co_{1-X}Mn_X)O_3$.

(8) The difference of spin state in Co^{3+} ion in $SrCoO_{3-\delta}$ and $(La_{1-X}Sr_X)CoO_3$ system suggested that A cation (Sr^{2+} and La^{3+} ions) played a significant role to the electron configuration of other cations.

(9) The magnetic and electrical properties for $SrCoO_{3-\delta}$ and $(La_{1-X}Sr_X)CoO_3$ were explained by an intermediate-spin model localized t_{2g} configuration on each cobalt and

an itinerant σ^* orbitals.

ACKNOWLEDGEMENTS

The author wishes to express his appreciation to Professor M. Koizumi at Osaka University for his continuous guidance in the course of this work and Professors S. Kawai and K. Kuwata at Osaka University for their valuable discussions.

The author also thanks to Assist. Professor M. Shimada and Professor F. Kanamaru at Osaka University for their advices and helpful discussions throughout this thesis.

Thanks are also due to all members of the laboratoies under the direction of Professors M. Koizumi and S. Kume at Osaka University for encouraging me to complete this thesis work.

REFERENCES

1. J.B.Macchesney, R.C.Sherwood and J.F.Potter, J. Chem. Phys., 43 1907 (1965)
2. H.Watanabe, J. Phys. Soc. Japan, 12 515 (1957)
3. J.J.Lander, Acta Cryst., 4 148 (1951)
4. H.L.Yakel, Acta Crtst., 8 394 (1955)
5. G.H.Jonker, Physica, 22 707 (1956)
6. J.B.Goodenough, J. Phys. Chem. Solid, 6 287 (1958)
7. G.H.Jonker, J. Appl. Phys., 37 1424 (1966)
8. L.Rimai and G.A.DeMars, Phys. Rev., 127 702 (1962)
9. R.T.Clevenger, J. Am. Cer. Soc., 46 207 (1963)
10. B.L.Chamberland and P.S.Danielson, J. Solid State Chem., 3 243 (1971)
11. J.B.Goodenough, Mat. Res. Bull., 6 967 (1971)
12. J.B.Goodenough, J.M.Longo and J.A.Kafalas, Mat. Res. Bull., 3 471 (1968)
13. B.L.Chamberland, Solid State Commun., 5 663 (1967)
14. J.B.MacChesney, H.J.Williams, J.F.Potter and R.C.Sherwood, Phys. Rev., 164 779 (1967)
15. T.Takeda and S.Ohara, J. Phys. Soc. Japan, 37 275 (1974)
16. F.Kanamaru, H.Miyamoto, Y.Mimura, M.Koizumi, M.Shimada and S.Kume, Mat. Res. Bull., 5 257 (1970)
17. Y.Takeda, S.Naka, M.Takano, T.Shinjo, T. Takada and M.Shimada, Mat. Res. Bull., 13 61 (1978)

18. T.Takeda, Y.Yamaguchi and H.Watanabe, J. Phys. Soc. Japan, 33 967 (1972)

19. H.Watanabe and T.Takeda, Proceeding International Conference of Ferrite, Kyoto. July 1970

20. T.Takeda and H.Watanabe, J. Phys. Soc. Japan, 33 973 (1972)

21. E.Bank and M.Mizushima, J. Appl. Phys., 40 1408 (1969)

22. G.H.Jonker and J.H.Van Santen, Physica, 19 120 (1953)

23. J.B.Goodenough, J. Phys. Chem. Solid, 6 287 (1958)

24. P.M.Raccah and J.B.Goodenough, J. Appl. Phys., 39 1209 (1968)

25. C.N.R.Rao, V.G.Bhide and N.F.Mott, Philos. Mag., 32 1277 (1975)

26. F.Askham, I.Frankuchen and R.Ward, J. Am. Chem. Soc., 72 3799 (1950)

27. V.G.Bhide, D.S.Rajoria, C.N.R.Rao, G.R.Rao and C.G.Jadhao, Phys. Rev., B12 2832 (1975)

28. P.K.Gallagher, J.B.MacChesney and D.N.E.Bachanan, J. Chem. Phys., 41 2429 (1964)

29. S.Kume, F.Kanamaru, Y.Shibasaki, M.Koizumi, K.Yasunami and T.Fukuda, Rev. Scientific Inst., 42 1856 (1971)

30. L.W.Finger, "A Fortran IV Computer Program for Structure Factor Calculation and Least-Square Refinement of Crystal Structure." (1972)

31. B.E.Gushee, L.Katz and R.Ward, J. Am. Chem. Soc., 5 5601 (1957)

32. R.M.Bozorth, "Ferromagnetism" (1951)

33. H.Taguchi, M.Shimada and M.Koizumi, J. Solid State Chem., 29 221 (1979)

34. T.Takeda, Y.Yamaguchi and H.Watanabe, J. Phys. Soc. Japan, 33 970 (1972)

35. H.Taguchi, M.Shimada and M.Koizumi, Mat. Res. Bull. (in contribution)

36. T.Shijo, M.Takano, H.Taguchi and M.Shimada, Proceeding Mossbauer Conference, Yugoslavia, 1979 (J. Physique, 1980) (in press)

37. H.Taguchi, M.Shimada and M.Koizumi, Mat. Res. Bull., 13 1225 (1978)

38. H.Taguchi, M.Shimada and M.Koizumi, J. Solid State Chem., 33 (1980) (in press)

39. H.Taguchi, M.Shimada, F.Kanamaru, M.Koizumi and Y.Takeda, J. Solid State Chem., 18 299 (1976)

40. H.Watanabe, J. Phys. Soc. Japan, 16 433 (1961)

41. H.Taguchi, M.Shimada, M.Koizumi and F.Kanamaru, J. Solid State Chem. (in contribution)

42. R.D.Shannon and C.T.Prewitt, Acta Cryst., B25 925 (1969)

43. H.Taguchi, Y.Takeda, F.Kanamaru, M.Shimada and M.Koizumi, Acta Cryst., B33 1299 (1977)

44. M.Shimada, Y.Takeda, H.Taguchi, F.Kanamaru and M.Koizumi, J. Cryst. Growth, 29 75 (1975)

45. P.M.Raccah and J.B.Goodenough, Phys. Rev., 155 932 (1967)

46. L.Cervinka, S.Krupicka and V.Synecek, J. Chem. Solid, 20 167 (1961)

47. J.Hinze and H.H.Joffe, Can. J. Chem., 41 1315 (1963)

48. L.Pauling, "The nature of the chemical bond." Cornell University Press (1960)

49. J.B.Goodenough and P.M.Raccah, J. Appl. Phys., 36 1031 (1965)

50. J.B.Goodenough, J. Appl. Phys., 37 1415 (1966)

51. J.B.Goodenough, Phys. Rev., 164 785 (1967)